

CERN-EP-2024-238
16 September 2024

Search for quasi-particle scattering in the quark–gluon plasma with jet splittings in pp and Pb–Pb collisions at $\sqrt{s_{\text{NN}}} = 5.02 \text{ TeV}$

ALICE Collaboration*

Abstract

The ALICE Collaboration reports measurements of the large relative transverse momentum (k_{T}) component of jet substructure in pp and in central and semicentral Pb–Pb collisions at center-of-mass energy per nucleon pair $\sqrt{s_{\text{NN}}} = 5.02 \text{ TeV}$. Enhancement in the yield of such large- k_{T} emissions in central Pb–Pb collisions is predicted to arise from partonic scattering with quasi-particles of the quark–gluon plasma. The analysis utilizes charged-particle jets reconstructed by the anti- k_{T} algorithm with resolution parameter $R = 0.2$ in the transverse-momentum interval $60 < p_{\text{T},\text{ch jet}} < 80 \text{ GeV}/c$. The soft drop and dynamical grooming algorithms are used to identify high transverse momentum splittings in the jet shower. Comparison of measurements in Pb–Pb and pp collisions shows medium-induced narrowing, corresponding to yield suppression of high- k_{T} splittings, in contrast to the expectation of yield enhancement due to quasi-particle scattering. The measurements are compared to theoretical model calculations incorporating jet quenching, both with and without quasi-particle scattering effects. These measurements provide new insight into the underlying mechanisms and theoretical modeling of jet quenching.

*This publication is dedicated to the memory of our colleague
Dr. Roy Crawford Lemmon who recently passed away*

Strongly-interacting matter at high temperature and density forms a deconfined state known as the quark–gluon plasma (QGP) [1, 2]. The QGP filled the universe a few microseconds after the Big Bang, and it is generated and studied today using high-energy nuclear collisions at the Relativistic Heavy-ion Collider (RHIC) and the Large Hadron Collider (LHC) [3–6]. RHIC and LHC measurements, together with theoretical studies, have revealed that the QGP exhibits marked emergent features; it flows with low specific viscosity and is opaque to the passage of energetic partons [7–9]. While static properties of the QGP can be calculated numerically using quantum chromodynamics (QCD) implemented on the lattice [10, 11], the microscopic mechanisms underlying these dynamic phenomena remain poorly understood.

In high-energy hadronic collisions, partons from the projectiles may scatter with high momentum transfer. Such scattered partons are initially highly virtual and evolve by radiating partons that hadronize in a collimated spray of particles which is observable experimentally, denoted a “jet.” The jet shower has rich internal substructure that is observable in correlations among its constituent particles. In pp collisions, jet production cross sections and substructure have been measured extensively [12–16]. Theoretical calculations at high perturbative order (pQCD) agree well with the measurements, which provide stringent tests of QCD [12, 15, 17–20]. Charged-particle jets are especially well suited for jet substructure measurement due to the excellent angular resolution of charged-particle tracking in modern particle detectors, and their properties are calculable in pQCD using non-perturbative track functions [21].

In collisions of heavy nuclei, jets are generated together with the QGP and interact with it. The interaction of a jet and the QGP, known as jet quenching, generates several observable phenomena: jet yield suppression, jet deflection, and modification of jet substructure [22, 23]. Jet quenching has been measured extensively at RHIC and the LHC with several different observables [24–34], providing incisive probes of the structure and dynamics of the QGP [35–38].

Jet scattering in the QGP may elucidate the microscopic structure of the medium and the nature of its constituent quasi-particles, in analogy to Rutherford scattering which revealed the nature of the atomic nucleus [39]. Rare, single-hard scattering off of medium constituents leads to a Coulomb-like power-law tail in the emission spectrum (Molière scattering) [40–42].

Two experimental approaches have been proposed to search for direct evidence of jet–QGP scattering: in-medium deflection of the jet centroid, which modifies the acoplanarity distribution [28, 29], and deflection of a component of the jet shower, resulting in the modification of jet internal structure [40, 41]. While significant medium-induced modification to acoplanarity distributions has recently been reported, the dependence of the modification on jet resolution parameter R indicates that it is due predominantly to medium response and energy redistribution, which mask the Molière-scattering signal [43–47]. For substructure observables, in-medium quasi-particle scattering corresponds to a relative increase in the rate of high transverse momentum splittings (high k_T) in the jet shower; to date, no search for Molière scattering in the QGP based on jet substructure has been reported.

This Letter reports the first measurement of medium-induced modification of jet substructure using high- k_T splittings to search for quasi-particle scattering in the quark–gluon plasma. The data were recorded by the ALICE Collaboration during LHC Run 2 for pp collisions and for central and semicentral Pb–Pb collisions at center-of-mass energy per nucleon pair $\sqrt{s_{NN}} = 5.02$ TeV. Charged-particle jets are reconstructed using the anti- k_T algorithm [48, 49] with resolution parameter $R = 0.2$ in the $60 < p_{T,\text{ch jet}} < 80$ GeV/ c jet transverse momentum interval. Background from the underlying event is corrected using constituent subtraction [50]. Jet substructure is measured using the soft drop [51] and dynamical grooming [52] algorithms. Theoretical calculations incorporating jet quenching are used to assess the effects of in-medium Molière scattering, and are compared to the data.

The ALICE detector and its performance are described in Refs. [5, 53, 54]. Event triggering and event characterization utilize the V0A and V0C scintillator detectors, which cover pseudorapidity intervals $2.8 < \eta < 5.1$ and $-3.7 < \eta < -1.7$, respectively [55], and the Zero Degree Calorimeters located ± 112.5

m along the beam axis from the nominal interaction point of the beams. Charged-particle tracking is carried out using signals from the Inner Tracking System (ITS) [56] and Time Projection Chamber (TPC) [57] (and Transition Radiation Detector (TRD) [58] in pp collisions). The tracking acceptance covers $|\eta| < 0.9$ over the full azimuth.

The dataset, triggering, and event selection for pp and Pb–Pb collisions at $\sqrt{s_{\text{NN}}} = 5.02$ TeV are identical to those of the analysis described in Ref. [31]. Data were recorded with a minimum bias trigger and an event-activity (EA) trigger based on the V0 signal. For the Pb–Pb analysis, events are selected within the 0–10% (“central”) and 30–50% (“semicentral”) decile bins in EA. After event selection the pp collision dataset comprises 870 million events, corresponding to integrated luminosity $\mathcal{L}_{\text{int}} = 18.0 \pm 0.4 \text{ nb}^{-1}$ [59], while the Pb–Pb dataset comprises 92 million central and 90 million semicentral events, corresponding to $\mathcal{L}_{\text{int}} = 0.12$ and 0.06 nb^{-1} , respectively, with approximately 3% uncertainty [60].

Charged-particle tracks accepted for the analysis have $p_{\text{T}} > 0.15 \text{ GeV}/c$. Due to the spatially non-uniform ITS response, which also varied during the data-taking period, different classes of tracks are combined to create a population of charged-particle tracks with approximately uniform azimuthal acceptance [61]. Accepted tracks have momentum resolution $\sigma(p_{\text{T}})/p_{\text{T}} \sim 1\%$ for track $p_{\text{T}} = 1 \text{ GeV}/c$ and 4% at track $p_{\text{T}} = 50 \text{ GeV}/c$.

Both the pp and Pb–Pb datasets are corrected using events simulated by the PYTHIA 8 generator [62] with the Monash 2013 tune [63], whose output is denoted “particle level.” These events are then passed through a detailed model of the ALICE apparatus using GEANT 3 [64] to simulate detector effects, and reconstructed with the same algorithms utilized for the event, track, and jet reconstruction of the data; such events are denoted “detector level.” For Pb–Pb collisions, detector-level events are additionally embedded into real Pb–Pb data to include the effect of background from the underlying event, and are referred to as “reconstructed level”.

Measurements in pp collisions are compared with particle-level calculations using the pp-collision mode of JEWEL [65, 66] and the Hybrid model [67], which are based on PYTHIA 6 [68] and PYTHIA 8, respectively, and the JETSCAPE PP19 tune [69] based on the vacuum mode of the MATTER model [70]. For Pb–Pb collisions, the data are compared to calculations incorporating jet quenching. JETSCAPE (v3.5 AA22 tune [71–73]) is a multi-stage calculation of the medium-modified parton shower with virtuality-dependent interactions, based on MATTER and LBT [74]. The Hybrid Model [41, 75] incorporates AdS-CFT-inspired partonic energy loss and a model of medium response (“wake”). JEWEL is based on the BDMPS energy loss formalism [76] within a medium modeled with a Bjorken expansion, with an option to explicitly account for the distribution of partons in the QGP which recoil from the jet-QGP interaction. JETSCAPE and JEWEL include Molière scattering, while the Hybrid Model can disable elastic 2 → 2 Molière scattering to isolate such scattering effects.

The large underlying-event (UE) background in measured data is characterized via the p_{T} density ρ and mass density ρ_m [33, 61]. This background is suppressed using event-by-event constituent subtraction [50] with maximum subtraction distance parameter $R_{\text{max}} = 0.1$, and p_{T} -weight $\alpha = 0$, which is applied prior to jet finding. No UE subtraction is applied in pp collisions. Jet clustering implemented in FastJet 3.3.3 [77] is carried out twice in each event: first applying the anti- k_{T} clustering algorithm [48, 49] with charged-particle tracks to reconstruct jet candidates, and then using the Cambridge–Aachen (CA) clustering algorithm [78] with jet constituents from selected jet candidates to examine the jet substructure.

The anti- k_{T} clustering utilizes jet resolution parameter $R = 0.2$ and the E -recombination scheme [48]. The pion mass is assumed for all tracks. Charged-particle jet candidates are required to have $40 \leq p_{\text{T},\text{ch,jet}} < 120 \text{ GeV}/c$, jet area $A_{\text{jet}} > 0.6 \pi R^2$ [79], and jet centroid $|\eta_{\text{jet}}| < 0.9 - R$, with the minimum $p_{\text{T},\text{ch,jet}}$ and area requirements applied to remove jet candidates arising from uncorrelated background. Jet candidates containing a constituent with $p_{\text{T}} > 100 \text{ GeV}/c$ are rejected due to reduced momentum resolution in this

region.

Jet grooming algorithms [80, 81] are used to remove soft, wide-angle radiation by unwinding the CA recombination tree, allowing the identification of hard splittings. At each recombination step the algorithm evaluates a specified grooming condition based on a “hardness measure,” either accepting and recording the splitting properties, or rejecting the splitting and following the harder subjet to the next splitting. We utilize two different grooming algorithms which select splittings in distinct but partially overlapping regions of phase space, which may probe Molière scattering in different ways.

For soft drop grooming (“SD”) [51], the hardness measure is the fraction of the momentum carried in the softer subjet, z , and the grooming condition is $z > z_{\text{cut}}(\Delta R/R)^\beta$, where ΔR is the angle between the subjets, and z_{cut} and β are parameters of the algorithm. Successive splittings are evaluated until one passes the grooming condition, which tags the event, or no splittings remain (untagged event). This analysis utilizes $z_{\text{cut}} = 0.2$ and $\beta = 0$ to preferentially select more symmetric splittings.

For dynamical grooming (“DyG”) [52], the hardness measure is $\kappa \propto z(1-z)p_{T,\text{split}}(\Delta R/R)^a$, where a is a tunable hardness parameter and $p_{T,\text{split}}$ is the transverse momentum of the parent splitting. There is no explicit grooming condition, in contrast to SD; rather, the splitting with the largest value of hardness measure is always selected. This analysis utilizes $a = 1.0$ to preferentially select high- k_T splittings which may not be selected by SD.

Single hard scatterings may generate hard parton shower splittings. In this analysis, jet grooming is used to search for such hard splittings using the distribution of the relative transverse momentum of each splitting,

$$k_T = p_{T,\text{subleading}} \sin \Delta R, \quad (1)$$

where $p_{T,\text{subleading}}$ is the transverse momentum of the softer subjet, $\Delta R = \sqrt{\Delta y^2 + \Delta \phi^2}$, and $\Delta \phi$ and Δy are the subjet azimuthal angle and rapidity differences. The splitting phase space is characterized by k_T and ΔR , which are used to construct the Lund Plane [82]. The value of the splitting selected by the grooming algorithm is denoted $k_{T,g}$.

The complex background in Pb–Pb collisions generates false jet shower branches which may mask physical jet splittings and the physical leading and subleading subjets, with the subleading subjet more susceptible to contamination [31, 83]. The probability to falsely tag a background splitting is determined using embedding [83]. Measurements with small R in non-central Pb–Pb collisions mitigate such effects.

The DyG algorithm is especially susceptible to selecting incorrectly identified subjets since it considers all iterative splittings, without imposing a hard cutoff in the grooming condition. This effect is mitigated for Pb–Pb collisions by requiring $k_{T,g}^{\text{meas.}} > 1 \text{ GeV}/c$ in semicentral and $k_{T,g}^{\text{meas.}} > 1.5 \text{ GeV}/c$ in central, where $k_{T,g}^{\text{meas.}}$ is the background-subtracted but otherwise uncorrected $k_{T,g}$ distribution. This requirement trades more limited kinematic reach for increased purity; for details see Appendix A.

This minimum $k_{T,g}^{\text{meas.}}$ requirement and the SD grooming condition similarly reduce soft contamination and improve tagging purity. For central Pb–Pb collisions, SD ($z_{\text{cut}} = 0.2$) and DyG ($a = 1.0$) with $k_{T,g}^{\text{meas.}}$ have a subleading subjet true tagging rate of $\sim 80 - 90\%$.

The $k_{T,g}$ distributions are corrected for background fluctuations and detector effects, including track p_T resolution and tracking inefficiency. A response matrix is constructed in Pb–Pb (pp) collisions by correlating a probe jet at particle level and reconstructed level (detector level), relating the $p_{T,\text{jet}}$ and $k_{T,g}$ distributions. The response matrix is used to perform 2D iterative Bayesian unfolding [84, 85] as implemented in RooUnfold [86]. The optimal iteration for unfolding regularization is chosen such that variation in the unfolded distribution for successive iterations is less than 1%. The iteration number for regularization, which is optimized for each grooming method and collision system, ranges from 6 to 11.

A closure test which varies analysis components with respect to their nominal values is utilized to assess the full analysis chain. Closure corresponds to consistency within statistical error of corrected spectra for the variant and nominal components. Component variations include regularization parameter, prior spectrum shape, and background contribution via a parameterized thermal model and embedding. Point-by-point excursions from the closure tests beyond 1σ statistical error contribute to the systematic uncertainty.

For Pb–Pb collisions, systematic uncertainty in the $k_{T,g}$ distribution arises from the unfolding procedure, tracking efficiency, generator dependence of the response matrix, subtraction of the underlying event, and non-closure of the unfolding procedure due to mis-tagged subjets. For pp collisions, systematic uncertainty arises from unfolding, tracking efficiency, and generator dependence.

Systematic uncertainties are quantified as described in Appendix B. The systematic uncertainty due to track selection and ITS–TPC track-matching efficiency uncertainty is determined by randomly rejecting tracks with a given probability, which is p_T -dependent in Pb–Pb collisions. Under- and over-subtraction of background is assessed by varying the constituent subtraction distance parameter R_{\max} . Systematic uncertainties in the unfolding procedure are evaluated by varying the regularization parameter, the minimum jet $p_{T,\text{ch,jet}}$ range, the $k_{T,g}$ binning, and the prior. Generator dependence of the corrections is evaluated by unfolding with an alternative response matrix constructed using HERWIG 7 [87, 88] in pp collisions and JEWEL without recoils in Pb–Pb collisions. The closure tests exhibit non-closure of up to 12% in a single bin, with largest non-closure in central Pb–Pb collisions. The magnitude of the non-closure is correlated with residual background contamination.

The various contributions to the systematic uncertainty are largely uncorrelated among each other and are added in quadrature. The cumulative systematic uncertainty has magnitude 8–32% for central Pb–Pb and 2–7% for pp collisions. The dominant uncertainties arise from the generator dependence of the corrections, subtraction, and non-closure for Pb–Pb collisions, and the generator dependence and tracking for pp collisions.

Figure 1 shows the corrected $k_{T,g}$ yield distributions measured in pp and in central and semicentral Pb–Pb collisions, using DyG ($a = 1.0$) (left) and SD ($z_{\text{cut}} = 0.2$) (right). Each distribution is normalized by the number of jets found in the $60 < p_{T,\text{ch,jet}} < 80$ GeV/c interval. This is the first measurement of heavy-ion collision data to employ DyG. All distributions have a similar shape, with a steeply decreasing slope for $k_{T,g} > 1$ GeV/c. The results from pp collisions show a maximum at $k_{T,g} \approx 0.5\text{--}1$ GeV/c. The DyG ($a = 1.0$) spectra in Pb–Pb collisions are restricted to $k_{T,g} > 2$ GeV/c ($k_{T,g} > 3$ GeV/c) in semicentral (central) collisions due to the minimum $k_{T,g}$ requirement discussed above. The SD ($z_{\text{cut}} = 0.2$) spectra from pp collisions exhibit larger yield at high $k_{T,g}$ than those from Pb–Pb collisions, while for DyG ($a = 1.0$), the pp and Pb–Pb spectra are consistent within uncertainties for $k_{T,g} > 2$ GeV/c where the Pb–Pb results are available. Comparing at fixed centrality and collision system, the DyG ($a = 1.0$) and SD ($z_{\text{cut}} = 0.2$) distributions are consistent over the measured $k_{T,g}$ range within the systematic error and statistical uncertainty.

Figure 2 shows the same distributions as Fig. 1, in this case as the ratio with a smooth function that parametrizes the data (details in Appendix C). This representation removes the main functional dependence on $k_{T,g}$ so that detailed variation of the distributions can be seen. The function parameters are different for each collision system, centrality class, and grooming method. Model calculations are also shown, and are divided by the same data parametrization. In the upper panels, the central values of the JETSCAPE and Hybrid Model calculations tend to underpredict the measured pp distribution at high k_T for both DyG ($a = 1.0$) and SD ($z_{\text{cut}} = 0.2$), though are consistent with the data within the uncertainties. At low $k_{T,g}$ (< 1 GeV/c), the JETSCAPE and Hybrid calculations with SD ($z_{\text{cut}} = 0.2$) grooming hint towards slightly overpredicting the data, while JEWEL underpredicts the DyG ($a = 1.0$) data. JEWEL overestimates the data at intermediate $k_{T,g}$ for both grooming methods. For semicentral Pb–Pb collisions,

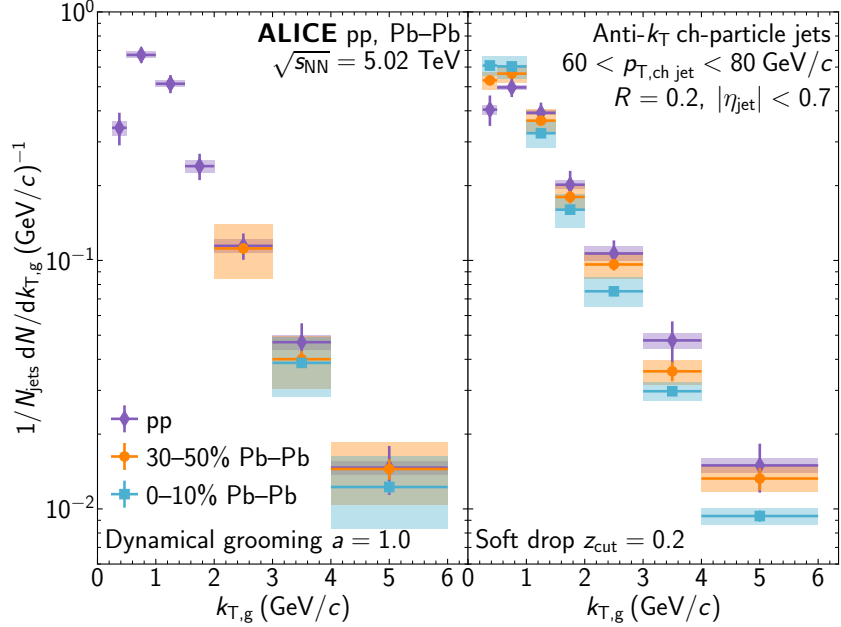


Figure 1: Unfolded $k_{T,g}$ spectra for splittings selected by dynamical grooming $a = 1.0$ (left) and soft drop $z_{\text{cut}} = 0.2$ (right) in pp and semicentral and central Pb–Pb collisions. The jets are measured with $R = 0.2$ in the $60 < p_{T,\text{ch jet}} < 80 \text{ GeV}/c$ interval. Statistical uncertainties are represented by bars, while systematic uncertainties are shown in shaded boxes.

displayed in the middle panels, both the DyG ($a = 1.0$) and SD ($z_{\text{cut}} = 0.2$) measurements are described well by all models for $k_{T,g} < 4 \text{ GeV}/c$. However, at high $k_{T,g}$, the Hybrid Model with Molière scattering (Hybrid/Molière) agrees better with the SD ($z_{\text{cut}} = 0.2$) data, while there is a hint that the other models underpredict the measured distributions. The bottom panels show tension of the models and data for SD ($z_{\text{cut}} = 0.2$) in central Pb–Pb collisions. At high $k_{T,g} > 3 \text{ GeV}/c$, the Hybrid Model without Molière scattering (Hybrid/noMolière) best describes the data, while Hybrid/Molière overpredicts, JETSCAPE slightly underpredicts, and JEWEL with and without recoils underpredict the measured values. For DyG ($a = 1.0$), Hybrid/Molière and Hybrid/noMolière best describe the data, while JETSCAPE and JEWEL underpredict the ratio. The large systematic uncertainties of the DyG ($a = 1.0$) spectra are due to a strong dependence of the grooming algorithm on the generator used to derive corrections of the spectra, limiting the model discrimination power. This indicates that the additional phase space probed by the algorithm does not provide further resolving power.

In-medium Molière scattering is expected to generate yield enhancement at large $k_{T,g}$ [40, 41], as seen in the Hybrid model variants in Fig 2. To search for this effect, Fig. 3 shows the ratios of $k_{T,g}$ distributions for semicentral and central Pb–Pb collisions to that for pp collisions. The SD ($z_{\text{cut}} = 0.2$) distributions exhibit medium-induced yield enhancement for $k_{T,g} < 1 \text{ GeV}/c$ and yield suppression at higher $k_{T,g}$, with stronger medium-induced effects in central than in semicentral Pb–Pb collisions. The DyG ($a = 1.0$) distributions hint at yield suppression at large $k_{T,g}$ for central Pb–Pb collisions but not for semicentral Pb–Pb collisions, though the ratios in both cases are consistent with unity within the systematic uncertainties. Since yield suppression is observed in the data in the high- $k_{T,g}$ region, this measurement does not show direct evidence of in-medium Molière scattering.

For SD ($z_{\text{cut}} = 0.2$) the central Pb–Pb/pp yield ratio is smaller than unity (where unity corresponds to the null hypothesis) by 3.1σ for $3 < k_{T,g} < 4 \text{ GeV}/c$ and by 2.6σ for $4 < k_{T,g} < 6 \text{ GeV}/c$ based on the statistical error, which is larger than the systematic uncertainty. This medium-induced narrowing of jet structure is qualitatively consistent with effects found in other inclusive jet substructure measurements [30, 31, 89]. Such narrowing is commonly interpreted as selection bias which modifies the relative fraction of quark-

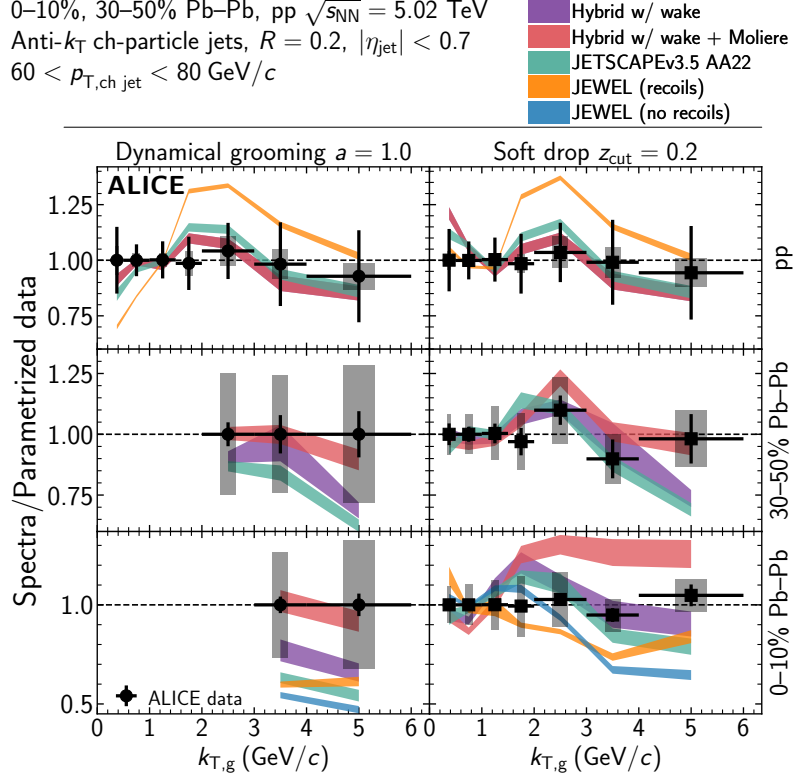


Figure 2: Ratio of $k_{T,g}$ distributions for data and model calculations to a smooth parametrization of the data, selected by dynamical grooming $a = 1.0$ (left) and soft drop $z_{\text{cut}} = 0.2$ (right). Data points are shown in black, with statistical (error bars) and systematic (grey boxes) uncertainties. The bands for the model calculations show statistical uncertainties.

or gluon-originating jets, due to the combined effects of a falling p_T spectrum and larger energy loss in the medium for wider jets [90–93]. The smaller modification of the $k_{T,g}$ distribution observed in semicentral Pb–Pb collisions is consistent with this picture, due to the correspondingly smaller jet energy loss in that population. The single-hard scattering signature may also be suppressed by subsequent multiple soft interactions with the medium, which smear the angular correlations of jet constituents, such that the Molière scattering is not reconstructed [94].

Figure 3 also shows model calculations. None of the models describe all measured distributions in Figs. 2 and 3, with different levels of agreement for the two grooming algorithms. The SD ($z_{\text{cut}} = 0.2$) analysis for central Pb–Pb collisions (Fig. 3, lower right) exhibits the most significant medium-induced modifications in this analysis, with experimental uncertainties which provide the best discrimination of model predictions. These data are well-described within uncertainties by JETSCAPE (with Molière scattering) and Hybrid/noMolière, but not by Hybrid/Molière or either variant of JEWEL. From this comparison it is evident that the different theoretical approaches of these models to jet quenching and the bulk dynamics of the QGP generate markedly different predictions for the relative effect of Molière scattering, which these and other recent data [44] can discriminate.

This Letter reports the first measurement of the distribution of the hardest relative transverse jet splitting, $k_{T,g}$, in pp and Pb–Pb collisions, to search for evidence of quasi-particle scattering in the quark–gluon plasma. The hardest splitting is identified using the soft drop and dynamical grooming algorithms, the latter for the first time in heavy-ion collisions. The high- $k_{T,g}$ yield in central Pb–Pb collisions is observed to be suppressed relative to that in pp collisions, consistent with in-medium narrowing effects seen in other jet substructure observables. No direct evidence is observed for in-medium quasi-particle scattering within the measured phase space. Model calculations can reproduce the measurements within

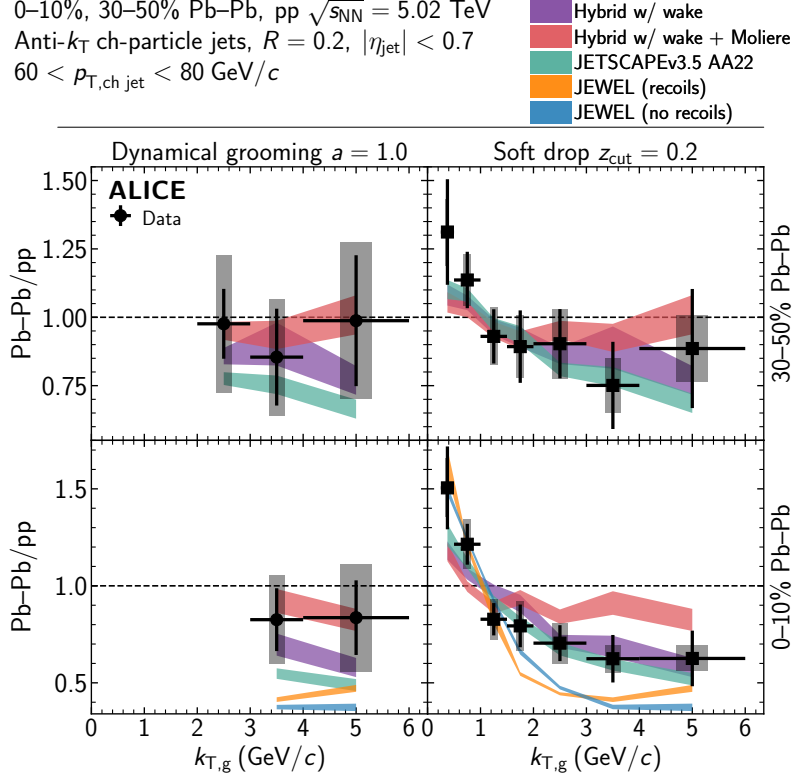


Figure 3: Ratio of the $k_{T,g}$ distributions measured in Pb–Pb and pp collisions for dynamical grooming $a = 1.0$ (left) and SD ($z_{\text{cut}} = 0.2$) (right), with comparison to model calculations. Statistical uncertainties are shown as error bars and systematic uncertainties are shown as grey shaded boxes for the measured ratios. The width of the colored bands corresponds to the statistical uncertainties in the model calculations.

uncertainties, but differ in the necessity to include quasi-particle scattering effects in order to do so. In these models, the Molière scattering signal may be masked by yield suppression due to jet energy loss, with their relative effects depending upon the theoretical picture underlying the modeling of jet quenching, bulk dynamics, and the vacuum parton shower. These data therefore provide new constraints on theoretical modeling of the microscopic structure and dynamics of the quark–gluon plasma.

Acknowledgements

We gratefully acknowledge Zach Hulcher and Daniel Pablos, and Yasuki Tachibana and the JETSCAPE collaboration, for providing calculations.

The ALICE Collaboration would like to thank all its engineers and technicians for their invaluable contributions to the construction of the experiment and the CERN accelerator teams for the outstanding performance of the LHC complex. The ALICE Collaboration gratefully acknowledges the resources and support provided by all Grid centres and the Worldwide LHC Computing Grid (WLCG) collaboration. The ALICE Collaboration acknowledges the following funding agencies for their support in building and running the ALICE detector: A. I. Alikhanyan National Science Laboratory (Yerevan Physics Institute) Foundation (ANSL), State Committee of Science and World Federation of Scientists (WFS), Armenia; Austrian Academy of Sciences, Austrian Science Fund (FWF): [M 2467-N36] and Nationalstiftung für Forschung, Technologie und Entwicklung, Austria; Ministry of Communications and High Technologies, National Nuclear Research Center, Azerbaijan; Conselho Nacional de Desenvolvimento Científico e Tecnológico (CNPq), Financiadora de Estudos e Projetos (Finep), Fundação de Amparo à Pesquisa do Estado de São Paulo (FAPESP) and Universidade Federal do Rio Grande do Sul (UFRGS),

Brazil; Bulgarian Ministry of Education and Science, within the National Roadmap for Research Infrastructures 2020-2027 (object CERN), Bulgaria; Ministry of Education of China (MOEC) , Ministry of Science & Technology of China (MSTC) and National Natural Science Foundation of China (NSFC), China; Ministry of Science and Education and Croatian Science Foundation, Croatia; Centro de Aplicaciones Tecnológicas y Desarrollo Nuclear (CEADEN), Cubaenergía, Cuba; Ministry of Education, Youth and Sports of the Czech Republic, Czech Republic; The Danish Council for Independent Research | Natural Sciences, the VILLUM FONDEN and Danish National Research Foundation (DNRF), Denmark; Helsinki Institute of Physics (HIP), Finland; Commissariat à l'Energie Atomique (CEA) and Institut National de Physique Nucléaire et de Physique des Particules (IN2P3) and Centre National de la Recherche Scientifique (CNRS), France; Bundesministerium für Bildung und Forschung (BMBF) and GSI Helmholtzzentrum für Schwerionenforschung GmbH, Germany; General Secretariat for Research and Technology, Ministry of Education, Research and Religions, Greece; National Research, Development and Innovation Office, Hungary; Department of Atomic Energy Government of India (DAE), Department of Science and Technology, Government of India (DST), University Grants Commission, Government of India (UGC) and Council of Scientific and Industrial Research (CSIR), India; National Research and Innovation Agency - BRIN, Indonesia; Istituto Nazionale di Fisica Nucleare (INFN), Italy; Japanese Ministry of Education, Culture, Sports, Science and Technology (MEXT) and Japan Society for the Promotion of Science (JSPS) KAKENHI, Japan; Consejo Nacional de Ciencia (CONACYT) y Tecnología, through Fondo de Cooperación Internacional en Ciencia y Tecnología (FONCICYT) and Dirección General de Asuntos del Personal Académico (DGAPA), Mexico; Nederlandse Organisatie voor Wetenschappelijk Onderzoek (NWO), Netherlands; The Research Council of Norway, Norway; Pontificia Universidad Católica del Perú, Peru; Ministry of Science and Higher Education, National Science Centre and WUT ID-UB, Poland; Korea Institute of Science and Technology Information and National Research Foundation of Korea (NRF), Republic of Korea; Ministry of Education and Scientific Research, Institute of Atomic Physics, Ministry of Research and Innovation and Institute of Atomic Physics and Universitatea Națională de Știință și Tehnologie Politehnica Bucuresti, Romania; Ministry of Education, Science, Research and Sport of the Slovak Republic, Slovakia; National Research Foundation of South Africa, South Africa; Swedish Research Council (VR) and Knut & Alice Wallenberg Foundation (KAW), Sweden; European Organization for Nuclear Research, Switzerland; Suranaree University of Technology (SUT), National Science and Technology Development Agency (NSTDA) and National Science, Research and Innovation Fund (NSRF via PMU-B B05F650021), Thailand; Turkish Energy, Nuclear and Mineral Research Agency (TENMAK), Turkey; National Academy of Sciences of Ukraine, Ukraine; Science and Technology Facilities Council (STFC), United Kingdom; National Science Foundation of the United States of America (NSF) and United States Department of Energy, Office of Nuclear Physics (DOE NP), United States of America. In addition, individual groups or members have received support from: Czech Science Foundation (grant no. 23-07499S), Czech Republic; FORTE project, reg. no. CZ.02.01.01/00/22_008/0004632, Czech Republic, co-funded by the European Union, Czech Republic; European Research Council (grant no. 950692), European Union; ICSC - Centro Nazionale di Ricerca in High Performance Computing, Big Data and Quantum Computing, European Union - NextGenerationEU; Academy of Finland (Center of Excellence in Quark Matter) (grant nos. 346327, 346328), Finland.

References

- [1] J. C. Collins and M. J. Perry, “Superdense matter: Neutrons or asymptotically free quarks?”, *Phys. Rev. Lett.* **34** (1975) 1353.
- [2] E. V. Shuryak, “Theory of hadronic plasma”, *Sov. Phys. JETP* **47** (1978) 212–219.
- [3] STAR Collaboration, J. Adams *et al.*, “Experimental and theoretical challenges in the search for

the quark gluon plasma: The STAR Collaboration’s critical assessment of the evidence from RHIC collisions”, *Nucl. Phys. A* **757** (2005) 102–183, arXiv:nucl-ex/0501009.

- [4] **PHENIX** Collaboration, K. Adcox *et al.*, “Formation of dense partonic matter in relativistic nucleus-nucleus collisions at RHIC: Experimental evaluation by the PHENIX collaboration”, *Nucl. Phys. A* **757** (2005) 184–283, arXiv:nucl-ex/0410003.
- [5] **ALICE** Collaboration, S. Acharya *et al.*, “The ALICE experiment – A journey through QCD”, *Eur. Phys. J. C* **84** (2024) 813, arXiv:2211.04384 [nucl-ex].
- [6] **CMS** Collaboration, A. Hayrapetyan *et al.*, “Overview of high-density QCD studies with the CMS experiment at the LHC”, arXiv:2405.10785 [nucl-ex].
- [7] B. V. Jacak and B. Müller, “The exploration of hot nuclear matter”, *Science* **337** (2012) 310–314.
- [8] W. Busza, K. Rajagopal, and W. van der Schee, “Heavy ion collisions: The big picture, and the big questions”, *Ann. Rev. Nucl. Part. Sci.* **68** (2018) 339–376, arXiv:1802.04801 [hep-ph].
- [9] J. W. Harris and B. Müller, “‘QGP signatures’ revisited”, *Eur. Phys. J. C* **84** (2023) 247, arXiv:2308.05743 [hep-ph].
- [10] C. Ratti, “Lattice QCD and heavy ion collisions: A review of recent progress”, *Rept. Prog. Phys.* **81** (2018) 084301, arXiv:1804.07810 [hep-lat].
- [11] J. N. Guenther, “Overview of the QCD phase diagram – recent progress from the lattice”, *Eur. Phys. J. A* **57** (2021) 136, arXiv:2010.15503 [hep-lat].
- [12] **ALICE** Collaboration, B. Abelev *et al.*, “Measurement of the inclusive differential jet cross section in pp collisions at $\sqrt{s} = 2.76$ TeV”, *Phys. Lett. B* **722** (2013) 262–272, arXiv:1301.3475 [nucl-ex].
- [13] **ATLAS** Collaboration, G. Aad *et al.*, “Jet mass and substructure of inclusive jets in $\sqrt{s} = 7$ TeV pp collisions with the ATLAS experiment”, *JHEP* **05** (2012) 128, arXiv:1203.4606 [hep-ex].
- [14] **CMS** Collaboration, A. Tumasyan *et al.*, “Measurement and QCD analysis of double-differential inclusive jet cross sections in proton-proton collisions at $\sqrt{s} = 13$ TeV”, *JHEP* **02** (2022) 142, arXiv:2111.10431 [hep-ex].
- [15] **ATLAS** Collaboration, G. Aad *et al.*, “Measurement of the Lund jet plane using charged particles in 13 TeV proton-proton collisions with the ATLAS detector”, *Phys. Rev. Lett.* **124** (2020) 222002, arXiv:2004.03540 [hep-ex].
- [16] **ALICE** Collaboration, S. Acharya *et al.*, “Measurements of the groomed jet radius and momentum splitting fraction with the soft drop and dynamical grooming algorithms in pp collisions at $\sqrt{s} = 5.02$ TeV”, *JHEP* **05** (2023) 244, arXiv:2204.10246 [hep-ex, physics:nucl-ex].
- [17] **STAR** Collaboration, B. Abelev *et al.*, “Longitudinal double-spin asymmetry and cross section for inclusive jet production in polarized proton collisions at $\sqrt{s} = 200$ GeV”, *Phys. Rev. Lett.* **97** (2006) 252001, arXiv:hep-ex/0608030.
- [18] **STAR** Collaboration, L. Adamczyk *et al.*, “Measurement of the cross section and longitudinal double-spin asymmetry for di-jet production in polarized pp collisions at $\sqrt{s} = 200$ GeV”, *Phys. Rev. D* **95** (2017) 071103, arXiv:1610.06616 [hep-ex].

- [19] **ATLAS** Collaboration, G. Aad *et al.*, “Measurement of the inclusive jet cross-section in proton-proton collisions at $\sqrt{s} = 7$ TeV using 4.5 fb^{-1} of data with the ATLAS detector”, *JHEP* **02** (2015) 153, arXiv:1410.8857 [hep-ex].
- [20] **CMS** Collaboration, V. Khachatryan *et al.*, “Measurement and QCD analysis of double-differential inclusive jet cross-sections in pp collisions at $\sqrt{s} = 8$ TeV and ratios to 2.76 and 7 TeV”, *JHEP* **03** (2017) 156, arXiv:1609.05331 [hep-ex].
- [21] K. Lee, I. Moult, F. Ringer, and W. J. Waalewijn, “A formalism for extracting track functions from jet measurements”, *JHEP* **01** (2024) 194, arXiv:2308.00028 [hep-ph].
- [22] L. Cunqueiro and A. M. Sickles, “Studying the QGP with jets at the LHC and RHIC”, *Prog. Part. Nucl. Phys.* **124** (2022) 103940, arXiv:2110.14490 [nucl-ex].
- [23] L. Apolinário, Y.-J. Lee, and M. Winn, “Heavy quarks and jets as probes of the QGP”, *Prog. Part. Nucl. Phys.* **127** (2022) 103990, arXiv:2203.16352 [hep-ph].
- [24] **STAR** Collaboration, J. Adam *et al.*, “Measurement of inclusive charged-particle jet production in Au+Au collisions at $\sqrt{s_{\text{NN}}}=200$ GeV”, *Phys. Rev. C* **102** (2020) 054913, arXiv:2006.00582 [nucl-ex].
- [25] **ALICE** Collaboration, S. Acharya *et al.*, “Measurement of the radius dependence of charged-particle jet suppression in Pb–Pb collisions at $\sqrt{s_{\text{NN}}} = 5.02$ TeV”, *Phys. Lett. B* **849** (2024) 138412, arXiv:2303.00592 [nucl-ex].
- [26] **ATLAS** Collaboration, M. Aaboud *et al.*, “Measurement of the nuclear modification factor for inclusive jets in Pb+Pb collisions at $\sqrt{s_{\text{NN}}} = 5.02$ TeV with the ATLAS detector”, *Phys. Lett. B* **790** (2019) 108–128, arXiv:1805.05635 [nucl-ex].
- [27] **CMS** Collaboration, A. M. Sirunyan *et al.*, “First measurement of large area jet transverse momentum spectra in heavy-ion collisions”, *JHEP* **05** (2021) 284, arXiv:2102.13080 [hep-ex].
- [28] **ALICE** Collaboration, J. Adam *et al.*, “Measurement of jet quenching with semi-inclusive hadron-jet distributions in central Pb–Pb collisions at $\sqrt{s_{\text{NN}}} = 2.76$ TeV”, *JHEP* **09** (2015) 170, arXiv:1506.03984 [nucl-ex].
- [29] **STAR** Collaboration, L. Adamczyk *et al.*, “Measurements of jet quenching with semi-inclusive hadron+jet distributions in Au+Au collisions at $\sqrt{s_{\text{NN}}} = 200$ GeV”, *Phys. Rev. C* **96** (2017) 024905, arXiv:1702.01108 [nucl-ex].
- [30] **ATLAS** Collaboration, G. Aad *et al.*, “Measurement of substructure-dependent jet suppression in Pb+Pb collisions at 5.02 TeV with the ATLAS detector”, *Phys. Rev. C* **107** (2023) 054909, arXiv:2211.11470 [nucl-ex].
- [31] **ALICE** Collaboration, S. Acharya *et al.*, “Measurement of the groomed jet radius and momentum splitting fraction in pp and Pb–Pb collisions at $\sqrt{s_{\text{NN}}} = 5.02$ TeV”, *Phys. Rev. Lett.* **128** (2022) 102001, arXiv:2107.12984 [nucl-ex].
- [32] **CMS** Collaboration, A. M. Sirunyan *et al.*, “Measurement of the groomed jet mass in PbPb and pp collisions at $\sqrt{s_{\text{NN}}} = 5.02$ TeV”, *JHEP* **10** (2018) 161, arXiv:1805.05145 [hep-ex].
- [33] **ALICE** Collaboration, S. Acharya *et al.*, “First measurement of jet mass in Pb–Pb and p–Pb collisions at the LHC”, *Phys. Lett. B* **776** (2018) 249–264, arXiv:1702.00804 [nucl-ex].

- [34] **ATLAS** Collaboration, G. Aad *et al.*, “Measurement of suppression of large-radius jets and its dependence on substructure in Pb+Pb collisions at $\sqrt{s_{\text{NN}}} = 5.02$ TeV with the ATLAS detector”, *Phys. Rev. Lett.* **131** (2023) 172301, arXiv:2301.05606 [nucl-ex].
- [35] **JET** Collaboration, K. M. Burke *et al.*, “Extracting the jet transport coefficient from jet quenching in high-energy heavy-ion collisions”, *Phys. Rev. C* **90** (2014) 014909, arXiv:1312.5003 [nucl-th].
- [36] **JETSCAPE** Collaboration, S. Cao *et al.*, “Determining the jet transport coefficient \hat{q} from inclusive hadron suppression measurements using Bayesian parameter estimation”, *Phys. Rev. C* **104** (2021) 024905, arXiv:2102.11337 [nucl-th].
- [37] **JETSCAPE** Collaboration, R. Ehlers *et al.*, “Bayesian Inference analysis of jet quenching using inclusive jet and hadron suppression measurements”, arXiv:2408.08247 [hep-ph].
- [38] W. Ke and X.-N. Wang, “QGP modification to single inclusive jets in a calibrated transport model”, *JHEP* **05** (2021) 041, arXiv:2010.13680 [hep-ph].
- [39] E. Rutherford, “The scattering of α and β particles by matter and the structure of the atom”, *Phil. Mag. Ser. 6* **21** (1911) 669–688, <https://doi.org/10.1080/14786440508637080>.
- [40] F. D’Eramo, M. Lekaveckas, H. Liu, and K. Rajagopal, “Momentum Broadening in Weakly Coupled Quark-Gluon Plasma (with a view to finding the quasiparticles within liquid quark-gluon plasma)”, *JHEP* **05** (2013) 031, arXiv:1211.1922 [hep-ph].
- [41] F. D’Eramo, K. Rajagopal, and Y. Yin, “Molière scattering in quark-gluon plasma: Finding point-like scatterers in a liquid”, *JHEP* **01** (2019) 172, arXiv:1808.03250 [hep-ph].
- [42] J. Barata, Y. Mehtar-Tani, A. Soto-Ontoso, and K. Tywoniuk, “Revisiting transverse momentum broadening in dense QCD media”, *Phys. Rev. D* **104** (2021) 054047, arXiv:2009.13667 [hep-ph].
- [43] **ALICE** Collaboration, S. Acharya *et al.*, “Measurements of jet quenching using semi-inclusive hadron+jet distributions in pp and central Pb–Pb collisions at $\sqrt{s_{\text{NN}}} = 5.02$ TeV”, *Phys. Rev. C* **110** (2024) 014906, arXiv:2308.16128 [nucl-ex].
- [44] **ALICE** Collaboration, S. Acharya *et al.*, “Observation of medium-induced yield enhancement and acoplanarity broadening of low- p_T jets from measurements in pp and central Pb–Pb collisions at $\sqrt{s_{\text{NN}}} = 5.02$ TeV”, *Phys. Rev. Lett.* **133** (2024) 022301, arXiv:2308.16131 [nucl-ex].
- [45] **STAR** Collaboration, M. Abdulhamid *et al.*, “Semi-inclusive direct photon+jet and π^0 +jet correlations measured in $p + p$ and central Au+Au collisions at $\sqrt{s_{\text{NN}}} = 200$ GeV”, arXiv:2309.00145 [nucl-ex].
- [46] **STAR** Collaboration, M. Abdulhamid *et al.*, “Measurement of in-medium jet modification using direct photon+jet and π^0 +jet correlations in $p + p$ and central Au+Au collisions at $\sqrt{s_{\text{NN}}} = 200$ GeV”, arXiv:2309.00156 [nucl-ex].
- [47] **CMS** Collaboration, A. M. Sirunyan *et al.*, “Study of jet quenching with isolated-photon+jet correlations in PbPb and pp collisions at $\sqrt{s_{\text{NN}}} = 5.02$ TeV”, *Phys. Lett. B* **785** (2018) 14–39, arXiv:1711.09738 [nucl-ex].
- [48] M. Cacciari, G. P. Salam, and G. Soyez, “The Catchment Area of Jets”, *JHEP* **04** (2008) 005, arXiv:0802.1188 [hep-ph].

- [49] M. Cacciari, G. P. Salam, and G. Soyez, “The anti- k_t jet clustering algorithm”, *JHEP* **04** (2008) 063, arXiv:0802.1189 [hep-ph].
- [50] P. Berta, M. Spousta, D. W. Miller, and R. Leitner, “Particle-level pileup subtraction for jets and jet shapes”, *JHEP* **06** (2014) 092, arXiv:1403.3108 [hep-ex].
- [51] A. J. Larkoski, S. Marzani, G. Soyez, and J. Thaler, “Soft Drop”, *JHEP* **05** (2014) 146, arXiv:1402.2657 [hep-ph].
- [52] Y. Mehtar-Tani, A. Soto-Ontoso, and K. Tywoniuk, “Dynamical grooming of QCD jets”, *Phys. Rev. D* **101** (2020) 034004, arXiv:1911.00375 [hep-ph].
- [53] ALICE Collaboration, K. Aamodt *et al.*, “The ALICE experiment at the CERN LHC”, *JINST* **3** (2008) S08002.
- [54] ALICE Collaboration, B. B. Abelev *et al.*, “Performance of the ALICE Experiment at the CERN LHC”, *Int. J. Mod. Phys. A* **29** (2014) 1430044, arXiv:1402.4476 [nucl-ex].
- [55] ALICE Collaboration, E. Abbas *et al.*, “Performance of the ALICE VZERO system”, *JINST* **8** (2013) P10016, arXiv:1306.3130 [nucl-ex].
- [56] ALICE Collaboration, K. Aamodt *et al.*, “Alignment of the ALICE Inner Tracking System with cosmic-ray tracks”, *JINST* **5** (2010) P03003, arXiv:1001.0502 [physics.ins-det].
- [57] J. Alme *et al.*, “The ALICE TPC, a large 3-dimensional tracking device with fast readout for ultra-high multiplicity events”, *Nucl. Instrum. Meth. A* **622** (2010) 316–367, arXiv:1001.1950 [physics.ins-det].
- [58] ALICE Collaboration, S. Acharya *et al.*, “The ALICE Transition Radiation Detector: Construction, operation, and performance”, *Nucl. Instrum. Meth. A* **881** (2018) 88–127, arXiv:1709.02743 [physics.ins-det].
- [59] ALICE Collaboration, S. Acharya *et al.*, “ALICE 2017 luminosity determination for pp collisions at $\sqrt{s} = 5$ TeV”, <http://cds.cern.ch/record/2648933>.
- [60] ALICE Collaboration, S. Acharya *et al.*, “ALICE luminosity determination for Pb–Pb collisions at $\sqrt{s_{\text{NN}}} = 5.02$ TeV”, *JINST* **19** (2024) P02039, arXiv:2204.10148 [nucl-ex].
- [61] ALICE Collaboration, B. Abelev *et al.*, “Measurement of event background fluctuations for charged particle jet reconstruction in Pb–Pb collisions at $\sqrt{s_{\text{NN}}} = 2.76$ TeV”, *JHEP* **03** (2012) 053, arXiv:1201.2423 [hep-ex].
- [62] T. Sjostrand *et al.*, “An introduction to PYTHIA 8.2”, *Comput. Phys. Commun.* **191** (2015) 159–177, arXiv:1410.3012 [hep-ph].
- [63] P. Skands, S. Carrazza, and J. Rojo, “Tuning PYTHIA 8.1: The Monash 2013 tune”, *Eur. Phys. J. C* **74** (2014) 3024, arXiv:1404.5630 [hep-ph].
- [64] R. Brun *et al.*, *GEANT: Detector Description and Simulation Tool; Oct 1994*. CERN Program Library. CERN, Geneva, 1993. <https://cds.cern.ch/record/1082634>. Long Writeup W5013.
- [65] K. C. Zapp, F. Krauss, and U. A. Wiedemann, “A perturbative framework for jet quenching”, *JHEP* **03** (2013) 080, arXiv:1212.1599 [hep-ph].
- [66] K. C. Zapp, “JEWEL 2.0.0 - Directions for Use”, *Eur. Phys. J. C* **74** (2014) 2762, arXiv:1311.0048 [hep-ph].

- [67] J. Casalderrey-Solana, D. C. Gulhan, J. G. Milhano, D. Pablos, and K. Rajagopal, “A hybrid strong/weak coupling approach to jet quenching”, *JHEP* **10** (2014) 019, arXiv:1405.3864 [hep-ph].
- [68] T. Sjostrand, S. Mrenna, and P. Skands, “PYTHIA 6.4 Physics and Manual”, *JHEP* **05** (2006) 026, arXiv:hep-ph/0603175.
- [69] **JETSCAPE** Collaboration, A. Kumar *et al.*, “The JETSCAPE framework: p+p results”, *Phys. Rev. C* **102** (2020) 054906, arXiv:1910.05481 [nucl-th].
- [70] S. Cao and A. Majumder, “Nuclear modification of leading hadrons and jets within a virtuality ordered parton shower”, *Phys. Rev. C* **101** (2020) 024903, arXiv:1712.10055 [nucl-th].
- [71] **JETSCAPE** Collaboration, J. Putschke *et al.*, “The JETSCAPE framework”, arXiv:1903.07706 [nucl-th].
- [72] **JETSCAPE** Collaboration, A. Kumar *et al.*, “Inclusive jet and hadron suppression in a multistage approach”, *Phys. Rev. C* **107** (2023) 034911, arXiv:2204.01163 [hep-ph].
- [73] **JETSCAPE** Collaboration, Y. Tachibana *et al.*, “Hard Jet Substructure in a Multi-stage Approach”, arXiv:2301.02485 [hep-ph].
- [74] Y. He, T. Luo, X.-N. Wang, and Y. Zhu, “Linear Boltzmann transport for jet propagation in the quark-gluon plasma: Elastic processes and medium recoil”, *Phys. Rev. C* **91** (2015) 054908, arXiv:1503.03313 [nucl-th].
- [75] Z. Hulcher, D. Pablos, and K. Rajagopal, “Resolution effects in the hybrid strong/weak coupling model”, *JHEP* **03** (2018) 010, arXiv:1707.05245 [hep-ph].
- [76] R. Baier, Y. L. Dokshitzer, A. H. Mueller, S. Peigne, and D. Schiff, “Radiative energy loss of high energy quarks and gluons in a finite-volume quark-gluon plasma”, *Nucl. Phys. B* **483** (1997) 291–320, arXiv:hep-ph/9607355.
- [77] M. Cacciari, G. P. Salam, and G. Soyez, “FastJet user manual”, *Eur. Phys. J. C* **72** (2012) 1896, arXiv:1111.6097 [hep-ph].
- [78] Y. L. Dokshitzer, G. D. Leder, S. Moretti, and B. R. Webber, “Better jet clustering algorithms”, *JHEP* **08** (1997) 001, arXiv:hep-ph/9707323.
- [79] **ALICE** Collaboration, B. Abelev *et al.*, “Measurement of charged jet suppression in Pb–Pb collisions at $\sqrt{s_{\text{NN}}} = 2.76$ TeV”, *JHEP* **03** (2014) 013, arXiv:1311.0633 [nucl-ex].
- [80] Y.-T. Chien and I. Vitev, “Probing the hardest branching of jets in heavy ion collisions”, *Phys. Rev. Lett.* **119** (2017) 112301, arXiv:1608.07283 [hep-ph].
- [81] Y. Mehtar-Tani and K. Tywoniuk, “Groomed jets in heavy-ion collisions: Sensitivity to medium-induced bremsstrahlung”, *JHEP* **04** (2017) 125, arXiv:1610.08930 [hep-ph].
- [82] H. A. Andrews *et al.*, “Novel tools and observables for jet physics in heavy-ion collisions”, *J. Phys. G* **47** (2020) 065102, arXiv:1808.03689 [hep-ph].
- [83] J. Mulligan and M. Ploskon, “Identifying groomed jet splittings in heavy-ion collisions”, *Phys. Rev. C* **102** (2020) 044913, arXiv:2006.01812 [hep-ph].
- [84] G. D’Agostini, “A multidimensional unfolding method based on Bayes’ theorem”, *Nucl. Instrum. Meth. A* **362** (1995) 487–498.

- [85] G. D'Agostini, “Improved iterative Bayesian unfolding”, in *Alliance Workshop on Unfolding and Data Correction*. 10, 2010. arXiv:1010.0632 [physics.data-an].
- [86] T. Adye, “Unfolding algorithms and tests using RooUnfold”, in *PHYSTAT 2011*, pp. 313–318. CERN, Geneva, 2011. arXiv:1105.1160 [physics.data-an].
- [87] M. Bahr *et al.*, “Herwig++ Physics and Manual”, *Eur. Phys. J. C* **58** (2008) 639–707, arXiv:0803.0883 [hep-ph].
- [88] J. Bellm *et al.*, “Herwig 7.0 / Herwig++ 3.0 Release Note”, *Eur. Phys. J. C* **76** (2016) 196, arXiv:1512.01178 [hep-ph].
- [89] ALICE Collaboration, S. Acharya *et al.*, “Measurement of the angle between jet axes in Pb–Pb collisions at $\sqrt{s_{\text{NN}}} = 5.02 \text{ TeV}$ ”, arXiv:2303.13347 [nucl-ex].
- [90] J. Casalderrey-Solana, D. Gulhan, G. Milhano, D. Pablos, and K. Rajagopal, “Angular structure of jet quenching within a hybrid strong/weak coupling model”, *JHEP* **03** (2017) 135, arXiv:1609.05842 [hep-ph].
- [91] F. Ringer, B.-W. Xiao, and F. Yuan, “Can we observe jet p_T -broadening in heavy-ion collisions at the LHC?”, *Phys. Lett. B* **808** (2020) 135634, arXiv:1907.12541 [hep-ph].
- [92] Y.-L. Du, D. Pablos, and K. Tywoniuk, “Deep learning jet modifications in heavy-ion collisions”, *JHEP* **21** (2020) 206, arXiv:2012.07797 [hep-ph].
- [93] J.-W. Kang, S. Wang, L. Wang, and B.-W. Zhang, “Phenomenological study of the angle between jet axes in heavy-ion collisions”, arXiv:2312.15518 [hep-ph].
- [94] Y. Mehtar-Tani, S. Schlichting, and I. Soudi, “Jet thermalization in QCD kinetic theory”, *JHEP* **05** (2023) 091, arXiv:2209.10569 [hep-ph].

End Matter

A Subjet purity

The large underlying event present in heavy-ion collisions contaminates the jet shower, leading to potential misidentification of physical jet splittings and the contributing subjets [31, 83]. For example, a true leading subjet may be paired with an uncorrelated jet constituent which is coincidentally close in angular phase space, leading to no hard splittings being identified in the declustering tree. Unlike algorithms with a hard cutoff in the grooming condition, DyG requires that a splitting be identified for each measured jet, even in the case that a jet is solely composed of soft splittings. The heavy background contamination of such soft splittings causes unfolding instabilities. These instabilities may be addressed via modifications to existing analysis procedures, which are explored below.

To characterize the impact of background contamination and study mitigation techniques, PYTHIA 8 probe jets generated with the Monash 2013 tune are embedded into Pb–Pb data, following a similar evaluation procedure as described in Ref. [83]. The grooming algorithms are applied to the probe jets at both the detector and reconstructed (i.e. embedded) levels. Performance is characterized by the purity, which is the fraction of subjets which are correctly identified in reconstructed-level jets, normalized by the number of groomed subjets found in detector-level jets. Identified splittings and subjets are matched based on subjet constituents, with the reconstructed-level subjet required to carry at least 50% of the detector-level subjet p_T . The leading subjet prong is correctly identified in more than 95% of all splittings, and is not shown here. The subleading subjet prong purity as a function of the detector-level probe $p_{T,\text{ch,jet}}$ is shown in Fig. A.1 for semicentral (left) and central (right) Pb–Pb collisions. Detector-level $p_{T,\text{ch,jet}}$ is utilized to assess the impact of background on the purity (as compared to detector effects). The $40 < p_{T,\text{ch,jet}}^{\text{det}} < 120 \text{ GeV}/c$ interval contains nearly all of the particle-level jets which contribute to the unfolded measurement. Soft drop $z_{\text{cut}} = 0.2$ correctly identifies more than 80% (90%) of subleading prongs in central (semicentral) Pb–Pb collisions. However, the purity drops to 65% (85%) for dynamical grooming $a = 1.0$, which leads to unfolding instabilities.

The subleading subjet purity can be improved by excluding the most background contaminated region of the $k_{T,g}$ spectra by requiring that the background-subtracted but otherwise uncorrected value, $k_{T,g}^{\text{meas.}}$, is larger than a minimum value. Figure A.1, open markers, demonstrates this effect, with the subleading subjet purity of dynamical grooming $a = 1.0$ with a minimum $k_{T,g}^{\text{meas.}}$ requirement increasing to near agreement with soft drop $z_{\text{cut}} = 0.2$. This requirement causes a corresponding reduction in the kinematic efficiency, which describes the efficiency of finding particle-level jets given a fixed detector-level kinematic interval [79], at low $k_{T,g} \sim 1\text{--}2 \text{ GeV}/c$. Reduced kinematic efficiency restricts the reported kinematic range to larger $k_{T,g}$ values where the kinematic efficiency is relatively higher, and increases sensitivity to the generator used to correct for this reduction. This analysis requires a kinematic efficiency greater than $\sim 70\%$. Optimizing the increase in purity against the reduction in kinematic efficiency (and therefore the reported kinematic range), $k_{T,g}^{\text{meas.}} > 1.5$ (1.0) GeV/c in central (semicentral) Pb–Pb collisions was selected for this measurement. Imposing this $k_{T,g}^{\text{meas.}}$ condition for soft drop $z_{\text{cut}} = 0.2$ does not improve the subleading subjet purity because the grooming condition already removes the background contamination.

B Systematic uncertainties

The systematic uncertainties in this measurement are due to the tracking efficiency, the subtraction of the underlying background, the unfolding procedure, the generator dependence of the unfolding procedure, and the residual non-closure of the unfolding procedure. Only the tracking, generator dependence, and unfolding apply to the measurement in pp collisions. Sources of uncertainty are evaluated following similar procedures and for similar physical considerations as described in Ref. [31]. Signed uncertainties are symmetrized. The total uncertainty is summed in quadrature over the sources mentioned above,

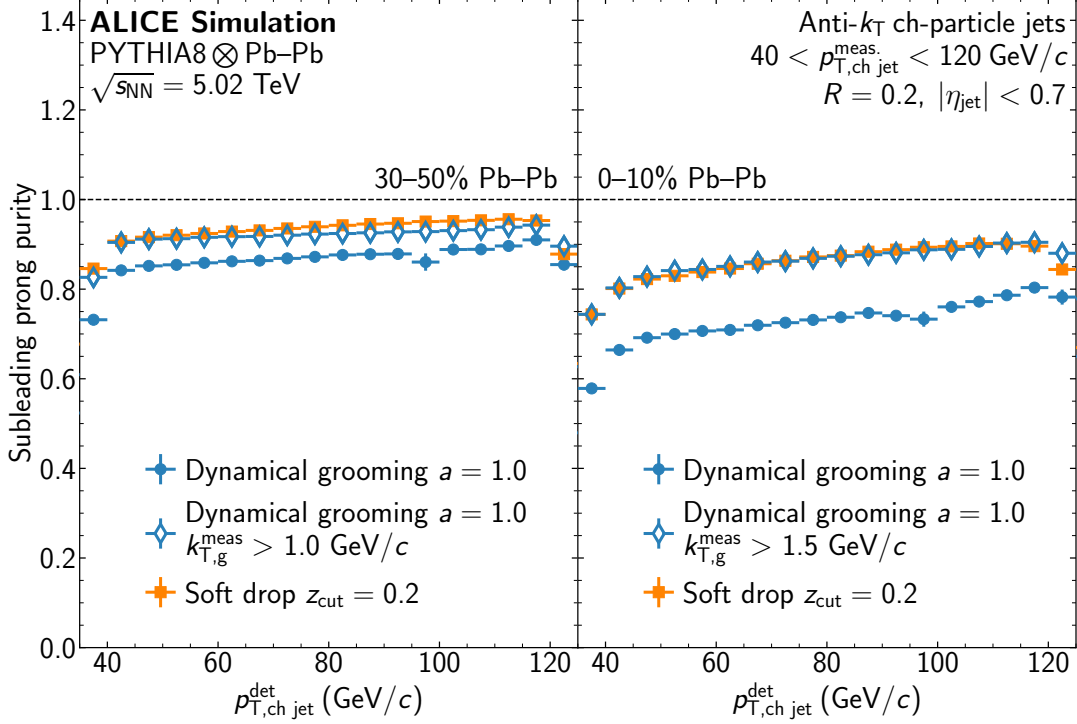


Figure A.1: Subleading subjet purity for soft drop $z_{\text{cut}} = 0.2$ and dynamical grooming $a = 1.0$ applied to jets found in semicentral (left) and central (right) Pb–Pb collisions. Closed markers correspond to the standard grooming algorithms, while open markers represent dynamical grooming $a = 1.0$ with a minimum $k_{T,g}^{\text{meas.}}$ requirement. Statistical uncertainties are represented by bars.

assuming no correlation between the individual uncertainties.

Track selections are considered along with the uncertainty on the ITS–TPC track-matching efficiency to estimate the systematic uncertainty on the observable due to the tracking performance. In pp collisions, this amounts to a p_{T} -independent uncertainty of $\sim 3\%$, while in Pb–Pb collisions, a p_{T} -dependent parametrization peaks at $\sim 6\%$ for $p_{\text{T}} = 1 \text{ GeV}/c$ and decreases to $\sim 3\%$ for $p_{\text{T}} \geq 15 \text{ GeV}/c$. This performance dependence is assessed by randomly rejecting tracks according to the magnitude of the uncertainties.

Imperfect background subtraction may bias the $p_{T,\text{ch jet}}$ and k_{T} dependence of the measured $k_{T,g}$ distributions. The analysis was carried out with two values of the constituent subtraction distance parameter R_{max} , 0.05 and 0.5, to characterize under- and over-subtraction of background contributions. The maximum bin-by-bin variation is assigned as a systematic uncertainty.

Sensitivity to the unfolding procedure is evaluated via variations of the unfolding parameters, including: varying the regularization parameter of the Bayesian unfolding by ± 1 unit; increasing and decreasing the minimum smeared jet $p_{T,\text{ch jet}}$ range by $\pm 5 \text{ GeV}/c$ in Pb–Pb collisions ($\pm 3 \text{ GeV}/c$ in pp collisions); modifying the $k_{T,g}$ bin edges by up to $\pm 5\%$; and weighing the prior distribution to resemble the uncorrected raw distributions. These variations are correlated in their characterization of the unfolding performance and sensitivity. Consequently, the variations are combined into a single unfolding uncertainty, calculated as the standard deviation of the individual values.

The generator utilized to construct the response matrix used for the unfolding can impact the measured distributions. This is evaluated by constructing alternative response matrices using HERWIG 7 [87, 88] in pp collisions, and JEWEL 2.2.0 [65, 66] without recoils in Pb–Pb collisions. A fast simulation is employed as described in Ref. [31], and the uncertainty is determined as the maximum bin-by-bin variation.

The systematic uncertainty derived in central collisions is also applied in semicentral collisions.

To account for the effects of residual subjet misidentifications, two methods are considered. Closure tests are performed using two approaches: 1) unfolding a known input distribution which is weighed to resemble the measured data; and 2) unfolding a known probe distribution which is embedded into a thermal background, as described in Ref. [31]. Any remaining non-closure in these correction procedures is taken as a systematic uncertainty, with the value assigned as the maximum bin-by-bin difference of the two methods from the nominal value.

Relative systematic uncertainties of $k_{T,g}$ distributions measured using soft drop $z_{\text{cut}} = 0.2$ and dynamical grooming $a = 1.0$ are shown in Table B.1 for pp collisions and Table B.2 for 0–10% and 30–50% Pb–Pb collisions.

Table B.1: Relative systematic uncertainties (%) for $k_{T,g}$ distributions measured using soft drop $z_{\text{cut}} = 0.2$ and dynamical grooming $a = 1.0$ in pp collisions. The minimum and maximum values over the measured $k_{T,g}$ range are reported. The combined uncertainty is the sum in quadrature of the individual uncertainties.

pp	Relative uncertainty (%)				
	Trk. Eff.	Generator	Unfolding	Total	
DyG. $a = 1.0$	1 – 6%	2 – 6%	1 – 4%	3 – 7%	
SD $z_{\text{cut}} = 0.2$	0 – 4%	1 – 6%	1 – 2%	2 – 7%	

Table B.2: Relative systematic uncertainties (%) for $k_{T,g}$ distributions measured using soft drop $z_{\text{cut}} = 0.2$ and dynamical grooming $a = 1.0$ in central and semicentral Pb–Pb collisions. The minimum and maximum values over the measured $k_{T,g}$ range are reported. The combined uncertainty is the sum in quadrature of the individual uncertainties.

Pb–Pb	Relative uncertainty (%)						
	Trk. Eff.	Bkgd. Sub.	Unfolding	Generator	Non-closure	Total	
DyG. $a = 1.0$	0–10%	4 – 7%	8 – 14%	1 – 2%	22 – 26%	12 – 12%	27 – 32%
SD $z_{\text{cut}} = 0.2$	0–10%	0 – 7%	1 – 7%	0 – 2%	2 – 11%	2 – 6%	8 – 15%
DyG. $a = 1.0$	30–50%	1 – 6%	4 – 9%	1 – 2%	22 – 26%	2 – 5%	24 – 28%
SD $z_{\text{cut}} = 0.2$	30–50%	0 – 5%	1 – 9%	0 – 2%	2 – 11%	1 – 5%	8 – 12%

C Parametrization of spectra

A smoothed parametrization was employed in order to factorize the overall features of the spectra while separating out the fluctuations of the data and model calculations. The smoothed functions were separately fit to the data in for each grooming method in pp, semicentral, and central Pb–Pb collisions. The same extracted parameters are used in the parametrized function to calculate the ratios with the data and the model calculations. The spectra are parametrized by

$$f(k_T, k_T^0, s) = [q(k_T, A, B) + (E - q(k_T^0, A, B))]t(k_T, k_T^0, -s) + [p(k_T, C, D) + (E - p(k_T^0, C, D))]t(k_T, k_T^0, s), \quad (\text{C.1})$$

with each term defined as,

$$\begin{aligned}
q(k_T; A, B) &= A(k_T - B)^2, \\
p(k_T; C, D) &= (Ck_T)^{-D}, \\
t(k_T; k_T^0, s) &= (1 + \tanh((k_T - k_T^0)/s))/2,
\end{aligned} \tag{C.2}$$

where A , B , C , D , and E are fit parameters, $s = 0.1$ for both grooming methods in Pb–Pb collisions, $s = 0.3$ for SD ($z_{\text{cut}} = 0.2$) and $s = 0.2$ for DyG ($a = 1.0$) in pp collisions, and $k_T^0 = 1.25 \text{ GeV}/c$. The particular functional forms are arbitrary; they were selected to provide a smooth approximate description of the bulk features of the spectra, with a peak at low $k_{T,g}$ via a quadratic term, transitioning to a power law at high $k_{T,g}$. For DyG ($a = 1.0$) in central Pb–Pb collisions, where there are insufficient points to constrain the high- $k_{T,g}$ fit, the $k_{T,g} = 2\text{--}3$ bin with low kinematic efficiency is included. The $1 + \tanh(\dots)$ element smoothly transitions between the two terms, while the normalization ensures that each term only contributes in its region of applicability.

D The ALICE Collaboration

S. Acharya ¹²⁷, A. Agarwal¹³⁵, G. Aglieri Rinella ³², L. Aglietta ²⁴, M. Agnello ²⁹, N. Agrawal ²⁵, Z. Ahammed ¹³⁵, S. Ahmad ¹⁵, S.U. Ahn ⁷¹, I. Ahuja ³⁷, A. Akindinov ¹⁴⁰, V. Akishina³⁸, M. Al-Turany ⁹⁷, D. Aleksandrov ¹⁴⁰, B. Alessandro ⁵⁶, H.M. Alfanda ⁶, R. Alfaro Molina ⁶⁷, B. Ali ¹⁵, A. Alici ²⁵, N. Alizadehvandchali ¹¹⁶, A. Alkin ¹⁰⁴, J. Alme ²⁰, G. Alocco ^{24,52}, T. Alt ⁶⁴, A.R. Altamura ⁵⁰, I. Altsybeev ⁹⁵, J.R. Alvarado ⁴⁴, C.O.R. Alvarez⁴⁴, M.N. Anaam ⁶, C. Andrei ⁴⁵, N. Andreou ¹¹⁵, A. Andronic ¹²⁶, E. Andronov ¹⁴⁰, V. Anguelov ⁹⁴, F. Antinori ⁵⁴, P. Antonioli ⁵¹, N. Apadula ⁷⁴, L. Aphecetche ¹⁰³, H. Appelshäuser ⁶⁴, C. Arata ⁷³, S. Arcelli ²⁵, R. Arnaldi ⁵⁶, J.G.M.C.A. Arneiro ¹¹⁰, I.C. Arsene ¹⁹, M. Arslanbekov ¹³⁸, A. Augustinus ³², R. Averbeck ⁹⁷, D. Averyanov ¹⁴⁰, M.D. Azmi ¹⁵, H. Baba¹²⁴, A. Badalà ⁵³, J. Bae ¹⁰⁴, Y.W. Baek ⁴⁰, X. Bai ¹²⁰, R. Bailhache ⁶⁴, Y. Bailung ⁴⁸, R. Bala ⁹¹, A. Balbino ²⁹, A. Baldissari ¹³⁰, B. Balis ², Z. Banoo ⁹¹, V. Barbasova³⁷, F. Barile ³¹, L. Barioglio ⁵⁶, M. Barlou⁷⁸, B. Barman⁴¹, G.G. Barnaföldi ⁴⁶, L.S. Barnby ¹¹⁵, E. Barreau ¹⁰³, V. Barret ¹²⁷, L. Barreto ¹¹⁰, C. Bartels ¹¹⁹, K. Barth ³², E. Bartsch ⁶⁴, N. Bastid ¹²⁷, S. Basu ⁷⁵, G. Batigne ¹⁰³, D. Battistini ⁹⁵, B. Batyunya ¹⁴¹, D. Bauri⁴⁷, J.L. Bazo Alba ¹⁰¹, I.G. Bearden ⁸³, C. Beattie ¹³⁸, P. Becht ⁹⁷, D. Behera ⁴⁸, I. Belikov ¹²⁹, A.D.C. Bell Hechavarria ¹²⁶, F. Bellini ²⁵, R. Bellwied ¹¹⁶, S. Belokurova ¹⁴⁰, L.G.E. Beltran ¹⁰⁹, Y.A.V. Beltran ⁴⁴, G. Bencedi ⁴⁶, A. Bensaoula¹¹⁶, S. Beole ²⁴, Y. Berdnikov ¹⁴⁰, A. Berdnikova ⁹⁴, L. Bergmann ⁹⁴, M.G. Besoiu ⁶³, L. Betev ³², P.P. Bhaduri ¹³⁵, A. Bhasin ⁹¹, B. Bhattacharjee ⁴¹, L. Bianchi ²⁴, J. Bielčík ³⁵, J. Bielčíková ⁸⁶, A.P. Bigot ¹²⁹, A. Bilandzic ⁹⁵, G. Biro ⁴⁶, S. Biswas ⁴, N. Bize ¹⁰³, J.T. Blair ¹⁰⁸, D. Blau ¹⁴⁰, M.B. Blidaru ⁹⁷, N. Bluhme³⁸, C. Blume ⁶⁴, G. Boca ^{21,55}, F. Bock ⁸⁷, T. Bodova ²⁰, J. Bok ¹⁶, L. Boldizsár ⁴⁶, M. Bombara ³⁷, P.M. Bond ³², G. Bonomi ^{134,55}, H. Borel ¹³⁰, A. Borissov ¹⁴⁰, A.G. Borquez Carcamo ⁹⁴, E. Botta ²⁴, Y.E.M. Bouziani ⁶⁴, L. Bratrud ⁶⁴, P. Braun-Munzinger ⁹⁷, M. Bregant ¹¹⁰, M. Broz ³⁵, G.E. Bruno ^{96,31}, V.D. Buchakchiev ³⁶, M.D. Buckland ⁸⁵, D. Budnikov ¹⁴⁰, H. Buesching ⁶⁴, S. Bufalino ²⁹, P. Buhler ¹⁰², N. Burmasov ¹⁴⁰, Z. Buthelezi ^{68,123}, A. Bylinkin ²⁰, S.A. Bysiak¹⁰⁷, J.C. Cabanillas Noris ¹⁰⁹, M.F.T. Cabrera¹¹⁶, M. Cai ⁶, H. Caines ¹³⁸, A. Caliva ²⁸, E. Calvo Villar ¹⁰¹, J.M.M. Camacho ¹⁰⁹, P. Camerini ²³, F.D.M. Canedo ¹¹⁰, S.L. Cantway ¹³⁸, M. Carabas ¹¹³, A.A. Carballo ³², F. Carnesecchi ³², R. Caron ¹²⁸, L.A.D. Carvalho ¹¹⁰, J. Castillo Castellanos ¹³⁰, M. Castoldi ³², F. Catalano ³², S. Cattaruzzi ²³, R. Cerri ²⁴, I. Chakaberia ⁷⁴, P. Chakraborty ¹³⁶, S. Chandra ¹³⁵, S. Chapelard ³², M. Chartier ¹¹⁹, S. Chattopadhyay¹³⁵, S. Chattopadhyay ¹³⁵, S. Chattopadhyay ⁹⁹, M. Chen³⁹, T. Cheng ⁶, C. Cheshkov ¹²⁸, V. Chibante Barroso ³², D.D. Chinellato ¹⁰², E.S. Chizzali ^{II,95}, J. Cho ⁵⁸, S. Cho ⁵⁸, P. Chochula ³², Z.A. Chochulska¹³⁶, D. Choudhury⁴¹, P. Christakoglou ⁸⁴, C.H. Christensen ⁸³, P. Christiansen ⁷⁵, T. Chujo ¹²⁵, M. Ciacco ²⁹, C. Cicalo ⁵², M.R. Ciupek⁹⁷, G. Clai^{III,51}, F. Colamaria ⁵⁰, J.S. Colburn¹⁰⁰, D. Colella ³¹, A. Colelli³¹, M. Colocci ²⁵, M. Concas ³², G. Conesa Balbastre ⁷³, Z. Conesa del Valle ¹³¹, G. Contin ²³, J.G. Contreras ³⁵, M.L. Coquet ¹⁰³, P. Cortese ^{133,56}, M.R. Cosentino ¹¹², F. Costa ³², S. Costanza ^{21,55}, C. Cot ¹³¹, P. Crochet ¹²⁷, L. Cunqueiro⁸⁷, M.M. Czarnynoga¹³⁶, A. Dainese ⁵⁴, G. Dange³⁸, M.C. Danisch ⁹⁴, A. Danu ⁶³, P. Das ⁸⁰, S. Das ⁴, A.R. Dash ¹²⁶, S. Dash ⁴⁷, A. De Caro ²⁸, G. de Cataldo ⁵⁰, J. de Cuveland³⁸, A. De Falco ²², D. De Gruttola ²⁸, N. De Marco ⁵⁶, C. De Martin ²³, S. De Pasquale ²⁸, R. Deb ¹³⁴, R. Del Grande ⁹⁵, L. Dello Stritto ³², W. Deng ⁶, K.C. Devereaux¹⁸, P. Dhankher ¹⁸, D. Di Bari ³¹, A. Di Mauro ³², B. Di Ruzza ¹³², B. Diab ¹³⁰, R.A. Diaz ^{141,7}, T. Dietel ¹¹⁴, Y. Ding ⁶, J. Ditzel ⁶⁴, R. Divià ³², Ø. Djupsland²⁰, U. Dmitrieva ¹⁴⁰, A. Dobrin ⁶³, B. Dönigus ⁶⁴, J.M. Dubinski ¹³⁶, A. Dubla ⁹⁷, P. Dupieux ¹²⁷, N. Dzalaiova¹³, T.M. Eder ¹²⁶, R.J. Ehlers ⁷⁴, F. Eisenhut ⁶⁴, R. Ejima ⁹², D. Elia ⁵⁰, B. Erazmus ¹⁰³, F. Ercolelli ²⁵, B. Espagnon ¹³¹, G. Elissee ³², D. Evans ¹⁰⁰, S. Evdokimov ¹⁴⁰, L. Fabbietti ⁹⁵, M. Faggion ²³, J. Faivre ⁷³, F. Fan ⁶, W. Fan ⁷⁴, A. Fantoni ⁴⁹, M. Fasel ⁸⁷, A. Feliciello ⁵⁶, G. Feofilov ¹⁴⁰, A. Fernández Téllez ⁴⁴, L. Ferrandi ¹¹⁰, M.B. Ferrer ³², A. Ferrero ¹³⁰, C. Ferrero ^{IV,56}, A. Ferretti ²⁴, V.J.G. Feuillard ⁹⁴, V. Filova ³⁵, D. Finogeev ¹⁴⁰, F.M. Fionda ⁵², E. Flatland³², F. Flor ^{138,116}, A.N. Flores ¹⁰⁸, S. Foertsch ⁶⁸, I. Fokin ⁹⁴, S. Fokin ¹⁴⁰, U. Follo ^{IV,56}, E. Fragiocomo ⁵⁷, E. Frajna ⁴⁶, U. Fuchs ³², N. Funicello ²⁸, C. Forget ⁷³, A. Furs ¹⁴⁰, T. Fusayasu ⁹⁸, J.J. Gaardhøje ⁸³, M. Gagliardi ²⁴, A.M. Gago ¹⁰¹, T. Gahlaud⁴⁷, C.D. Galvan ¹⁰⁹, S. Gami⁸⁰, D.R. Gangadhara ¹¹⁶, P. Ganoti ⁷⁸, C. Garabatos ⁹⁷, J.M. Garcia⁴⁴, T. García Chávez ⁴⁴, E. Garcia-Solis ⁹, C. Gargiulo ³², P. Gasik ⁹⁷, H.M. Gaur ³⁸, A. Gautam ¹¹⁸, M.B. Gay Ducati ⁶⁶, M. Germain ¹⁰³, R.A. Gernhaeuser⁹⁵, C. Ghosh¹³⁵, M. Giacalone ⁵¹, G. Gioachin ²⁹, S.K. Giri¹³⁵, P. Giubellino ^{97,56}, P. Giubilato ²⁷, A.M.C. Glaenzer ¹³⁰, P. Glässel ⁹⁴, E. Glimos ¹²², D.J.Q. Goh⁷⁶, V. Gonzalez ¹³⁷, P. Gordeev ¹⁴⁰, M. Gorgon ², K. Goswami ⁴⁸, S. Gotovac³³, V. Grabski ⁶⁷, L.K. Graczykowski ¹³⁶, E. Grecka ⁸⁶,

- A. Grelli ⁵⁹, C. Grigoras ³², V. Grigoriev ¹⁴⁰, S. Grigoryan ^{141,1}, F. Grossa ³²,
 J.F. Grosse-Oetringhaus ³², R. Grossi ⁹⁷, D. Grund ³⁵, N.A. Grunwald ⁹⁴, G.G. Guardiano ¹¹¹,
 R. Guernane ⁷³, M. Guilbaud ¹⁰³, K. Gulbrandsen ⁸³, J.J.W.K. Gumprecht ¹⁰², T. Gündem ⁶⁴,
 T. Gunji ¹²⁴, W. Guo ⁶, A. Gupta ⁹¹, R. Gupta ⁹¹, R. Gupta ⁴⁸, K. Gwizdziel ¹³⁶, L. Gyulai ⁴⁶,
 C. Hadjidakis ¹³¹, F.U. Haider ⁹¹, S. Haidlova ³⁵, M. Haldar ⁴, H. Hamagaki ⁷⁶, Y. Han ¹³⁹,
 B.G. Hanley ¹³⁷, R. Hannigan ¹⁰⁸, J. Hansen ⁷⁵, M.R. Haque ⁹⁷, J.W. Harris ¹³⁸, A. Harton ⁹,
 M.V. Hartung ⁶⁴, H. Hassan ¹¹⁷, D. Hatzifotiadou ⁵¹, P. Hauer ⁴², L.B. Havener ¹³⁸, E. Hellbär ³²,
 H. Helstrup ³⁴, M. Hemmer ⁶⁴, T. Herman ³⁵, S.G. Hernandez ¹¹⁶, G. Herrera Corral ⁸, S. Herrmann ¹²⁸,
 K.F. Hetland ³⁴, B. Heybeck ⁶⁴, H. Hillemanns ³², B. Hippolyte ¹²⁹, I.P.M. Hobus ⁸⁴, F.W. Hoffmann ⁷⁰,
 B. Hofman ⁵⁹, G.H. Hong ¹³⁹, M. Horst ⁹⁵, A. Horzyk ², Y. Hou ⁶, P. Hristov ³², P. Huhn ⁶⁴,
 L.M. Huhta ¹¹⁷, T.J. Humanic ⁸⁸, A. Hutson ¹¹⁶, D. Hutter ³⁸, M.C. Hwang ¹⁸, R. Ilkaev ¹⁴⁰,
 M. Inaba ¹²⁵, G.M. Innocent ³², M. Ippolitov ¹⁴⁰, A. Isakov ⁸⁴, T. Isidori ¹¹⁸, M.S. Islam ⁹⁹,
 S. Iurchenko ¹⁴⁰, M. Ivanov ⁹⁷, M. Ivanov ¹³, V. Ivanov ¹⁴⁰, K.E. Iversen ⁷⁵, M. Jablonski ²,
 B. Jacak ^{18,74}, N. Jacazio ²⁵, P.M. Jacobs ⁷⁴, S. Jadlovska ¹⁰⁶, J. Jadlovsky ¹⁰⁶, S. Jaelani ⁸², C. Jahnke ¹¹⁰,
 M.J. Jakubowska ¹³⁶, M.A. Janik ¹³⁶, T. Janson ⁷⁰, S. Ji ¹⁶, S. Jia ¹⁰, T. Jiang ¹⁰, A.A.P. Jimenez ⁶⁵,
 F. Jonas ⁷⁴, D.M. Jones ¹¹⁹, J.M. Jowett ^{32,97}, J. Jung ⁶⁴, M. Jung ⁶⁴, A. Junique ³², A. Jusko ¹⁰⁰,
 J. Kaewjai ¹⁰⁵, P. Kalinak ⁶⁰, A. Kalweit ³², A. Karasu Uysal ^{V,72}, D. Karatovic ⁸⁹, N. Karatzenis ¹⁰⁰,
 O. Karavichev ¹⁴⁰, T. Karavicheva ¹⁴⁰, E. Karpechev ¹⁴⁰, M.J. Karwowska ^{32,136}, U. Kebschull ⁷⁰,
 M. Keil ³², B. Ketzer ⁴², J. Keul ⁶⁴, S.S. Khade ⁴⁸, A.M. Khan ¹²⁰, S. Khan ¹⁵, A. Khanzadeev ¹⁴⁰,
 Y. Kharlov ¹⁴⁰, A. Khatun ¹¹⁸, A. Khuntia ³⁵, Z. Khuranova ⁶⁴, B. Kileng ³⁴, B. Kim ¹⁰⁴, C. Kim ¹⁶,
 D.J. Kim ¹¹⁷, E.J. Kim ⁶⁹, J. Kim ¹³⁹, J. Kim ⁵⁸, J. Kim ^{32,69}, M. Kim ¹⁸, S. Kim ¹⁷, T. Kim ¹³⁹,
 K. Kimura ⁹², A. Kirkova ³⁶, S. Kirsch ⁶⁴, I. Kisiel ³⁸, S. Kiselev ¹⁴⁰, A. Kisiel ¹³⁶, J.P. Kitowski ²,
 J.L. Klay ⁵, J. Klein ³², S. Klein ⁷⁴, C. Klein-Bösing ¹²⁶, M. Kleiner ⁶⁴, T. Klemenz ⁹⁵, A. Kluge ³²,
 C. Kobdaj ¹⁰⁵, R. Kohara ¹²⁴, T. Kollegger ⁹⁷, A. Kondratyev ¹⁴¹, N. Kondratyeva ¹⁴⁰, J. Konig ⁶⁴,
 S.A. Konigstorfer ⁹⁵, P.J. Konopka ³², G. Kornakov ¹³⁶, M. Korwieser ⁹⁵, S.D. Koryciak ², C. Koster ⁸⁴,
 A. Kotliarov ⁸⁶, N. Kovacic ⁸⁹, V. Kovalenko ¹⁴⁰, M. Kowalski ¹⁰⁷, V. Kozhuharov ³⁶, G. Kozlov ³⁸,
 I. Králik ⁶⁰, A. Kravčáková ³⁷, L. Krcal ^{32,38}, M. Krivda ^{100,60}, F. Krizek ⁸⁶, K. Krizkova Gajdosova ³²,
 C. Krug ⁶⁶, M. Krüger ⁶⁴, D.M. Krupova ³⁵, E. Kryshen ¹⁴⁰, V. Kučera ⁵⁸, C. Kuhn ¹²⁹,
 P.G. Kuijer ⁸⁴, T. Kumaoka ¹²⁵, D. Kumar ¹³⁵, L. Kumar ⁹⁰, N. Kumar ⁹⁰, S. Kumar ⁵⁰, S. Kundu ³²,
 P. Kurashvili ⁷⁹, A.B. Kurepin ¹⁴⁰, A. Kuryakin ¹⁴⁰, S. Kushpil ⁸⁶, V. Kuskov ¹⁴⁰, M. Kutyla ¹³⁶,
 A. Kuznetsov ¹⁴¹, M.J. Kweon ⁵⁸, Y. Kwon ¹³⁹, S.L. La Pointe ³⁸, P. La Rocca ²⁶, A. Lakrathok ¹⁰⁵,
 M. Lamanna ³², A.R. Landou ⁷³, R. Langoy ¹²¹, P. Larionov ³², E. Laudi ³², L. Lautner ^{32,95},
 R.A.N. Laveaga ¹⁰⁹, R. Lavicka ¹⁰², R. Lea ^{134,55}, H. Lee ¹⁰⁴, I. Legrand ⁴⁵, G. Legras ¹²⁶,
 J. Lehrbach ³⁸, A.M. Lejeune ³⁵, T.M. Lelek ², R.C. Lemmon ^{I,85}, I. León Monzón ¹⁰⁹, M.M. Lesch ⁹⁵,
 E.D. Lesser ¹⁸, P. Lévai ⁴⁶, M. Li ⁶, P. Li ¹⁰, X. Li ¹⁰, B.E. Liang-gilman ¹⁸, J. Lien ¹²¹, R. Lietava ¹⁰⁰,
 I. Likmeta ¹¹⁶, B. Lim ²⁴, S.H. Lim ¹⁶, V. Lindenstruth ³⁸, C. Lippmann ⁹⁷, D.H. Liu ⁶, J. Liu ¹¹⁹,
 G.S.S. Liveraro ¹¹¹, I.M. Lofnes ²⁰, C. Loizides ⁸⁷, S. Lokos ¹⁰⁷, J. Lömkner ⁵⁹, X. Lopez ¹²⁷, E. López
 Torres ⁷, C. Lotteau ¹²⁸, P. Lu ^{97,120}, Z. Lu ¹⁰, F.V. Lugo ⁶⁷, J.R. Luhder ¹²⁶, M. Lunardon ²⁷,
 G. Luparello ⁵⁷, Y.G. Ma ³⁹, M. Mager ³², A. Maire ¹²⁹, E.M. Majerz ², M.V. Makarieva ³⁶,
 M. Malaev ¹⁴⁰, G. Malfattore ²⁵, N.M. Malik ⁹¹, S.K. Malik ⁹¹, L. Malinina ^{I,VIII,141}, D. Mallick ¹³¹,
 N. Mallick ⁴⁸, G. Mandaglio ^{30,53}, S.K. Mandal ⁷⁹, A. Manea ⁶³, V. Manko ¹⁴⁰, F. Manso ¹²⁷,
 V. Manzari ⁵⁰, Y. Mao ⁶, R.W. Marcjan ², G.V. Margagliotti ²³, A. Margotti ⁵¹, A. Marín ⁹⁷,
 C. Markert ¹⁰⁸, C.F.B. Marquez ³¹, P. Martinengo ³², M.I. Martínez ⁴⁴, G. Martínez García ¹⁰³,
 M.P.P. Martins ¹¹⁰, S. Masciocchi ⁹⁷, M. Masera ²⁴, A. Masoni ⁵², L. Massacrier ¹³¹, O. Massen ⁵⁹,
 A. Mastroserio ^{132,50}, O. Matonoha ⁷⁵, S. Mattiazzzo ²⁷, A. Matyja ¹⁰⁷, F. Mazzaschi ^{32,24},
 M. Mazzilli ¹¹⁶, Y. Melikyan ⁴³, M. Melo ¹¹⁰, A. Menchaca-Rocha ⁶⁷, J.E.M. Mendez ⁶⁵,
 E. Meninno ¹⁰², A.S. Menon ¹¹⁶, M.W. Menzel ^{32,94}, M. Meres ¹³, Y. Miake ¹²⁵, L. Micheletti ³²,
 D. Mihai ¹¹³, D.L. Mihaylov ⁹⁵, K. Mikhaylov ^{141,140}, N. Minafra ¹¹⁸, D. Miśkowiec ⁹⁷, A. Modak ¹³⁴,
 B. Mohanty ⁸⁰, M. Mohisin Khan ^{VI,15}, M.A. Molander ⁴³, S. Monira ¹³⁶, C. Mordasini ¹¹⁷, D.A. Moreira
 De Godoy ¹²⁶, I. Morozov ¹⁴⁰, A. Morsch ³², T. Mrnjavac ³², V. Muccifora ⁴⁹, S. Muhuri ¹³⁵,
 J.D. Mulligan ⁷⁴, A. Mulliri ²², M.G. Munhoz ¹¹⁰, R.H. Munzer ⁶⁴, H. Murakami ¹²⁴, S. Murray ¹¹⁴,
 L. Musa ³², J. Musinsky ⁶⁰, J.W. Myrcha ¹³⁶, B. Naik ¹²³, A.I. Nambrath ¹⁸, B.K. Nandi ⁴⁷,
 R. Nania ⁵¹, E. Nappi ⁵⁰, A.F. Nassirpour ¹⁷, V. Nastase ¹¹³, A. Nath ⁹⁴, S. Nath ¹³⁵, C. Nattrass ¹²²,
 M.N. Naydenov ³⁶, A. Neagu ¹⁹, A. Negru ¹¹³, E. Nekrasova ¹⁴⁰, L. Nellen ⁶⁵, R. Nepeivoda ⁷⁵, S. Nese ¹⁹,
 N. Nicassio ⁵⁰, B.S. Nielsen ⁸³, E.G. Nielsen ⁸³, S. Nikolaev ¹⁴⁰, S. Nikulin ¹⁴⁰, V. Nikulin ¹⁴⁰,
 F. Noferini ⁵¹, S. Noh ¹², P. Nomokonov ¹⁴¹, J. Norman ¹¹⁹, N. Novitzky ⁸⁷, P. Nowakowski ¹³⁶,

- A. Nyanin ¹⁴⁰, J. Nystrand ²⁰, S. Oh ¹⁷, A. Ohlson ⁷⁵, V.A. Okorokov ¹⁴⁰, J. Oleniacz ¹³⁶,
 A. Onnerstad ¹¹⁷, C. Oppedisano ⁵⁶, A. Ortiz Velasquez ⁶⁵, J. Otwinowski ¹⁰⁷, M. Oya ⁹², K. Oyama ⁷⁶,
 Y. Pachmayer ⁹⁴, S. Padhan ⁴⁷, D. Pagano ^{134,55}, G. Paić ⁶⁵, S. Paisano-Guzmán ⁴⁴, A. Palasciano ⁵⁰,
 I. Panasenko ⁷⁵, S. Panebianco ¹³⁰, C. Pantouvakis ²⁷, H. Park ¹²⁵, H. Park ¹⁰⁴, J. Park ¹²⁵,
 J.E. Parkkila ³², Y. Patley ⁴⁷, R.N. Patra ⁵⁰, B. Paul ¹³⁵, H. Pei ⁶, T. Peitzmann ⁵⁹, X. Peng ¹¹,
 M. Pennisi ²⁴, S. Perciballi ²⁴, D. Peresunko ¹⁴⁰, G.M. Perez ⁷, Y. Pestov ¹⁴⁰, M.T. Petersen ⁸³,
 V. Petrov ¹⁴⁰, M. Petrovici ⁴⁵, S. Piano ⁵⁷, M. Pikna ¹³, P. Pillot ¹⁰³, O. Pinazza ^{51,32}, L. Pinsky ¹¹⁶,
 C. Pinto ⁹⁵, S. Pisano ⁴⁹, M. Płoskoń ⁷⁴, M. Planinic ⁸⁹, F. Pliquet ⁶⁴, D.K. Plociennik ²,
 M.G. Poghosyan ⁸⁷, B. Polichtchouk ¹⁴⁰, S. Politano ²⁹, N. Poljak ⁸⁹, A. Pop ⁴⁵,
 S. Porteboeuf-Houssais ¹²⁷, V. Pozdniakov ^{I,141}, I.Y. Pozos ⁴⁴, K.K. Pradhan ⁴⁸, S.K. Prasad ⁴,
 S. Prasad ⁴⁸, R. Preghenella ⁵¹, F. Prino ⁵⁶, C.A. Pruneau ¹³⁷, I. Pshenichnov ¹⁴⁰, M. Puccio ³²,
 S. Pucillo ²⁴, S. Qiu ⁸⁴, L. Quaglia ²⁴, A.M.K. Radhakrishnan ⁴⁸, S. Ragoni ¹⁴, A. Rai ¹³⁸,
 A. Rakotozafindrabe ¹³⁰, L. Ramello ^{133,56}, F. Rami ¹²⁹, M. Rasa ²⁶, S.S. Räsänen ⁴³, R. Rath ⁵¹,
 M.P. Rauch ²⁰, I. Ravasenga ³², K.F. Read ^{87,122}, C. Reckziegel ¹¹², A.R. Redelbach ³⁸,
 K. Redlich ^{VII,79}, C.A. Reetz ⁹⁷, H.D. Regules-Medel ⁴⁴, A. Rehman ²⁰, F. Reidt ³², H.A. Reme-Ness ³⁴,
 K. Reygers ⁹⁴, A. Riabov ¹⁴⁰, V. Riabov ¹⁴⁰, R. Ricci ²⁸, M. Richter ²⁰, A.A. Riedel ⁹⁵,
 W. Riegler ³², A.G. Riffero ²⁴, M. Rignanese ²⁷, C. Ripoli ²⁸, C. Ristea ⁶³, M.V. Rodriguez ³²,
 M. Rodríguez Cahuantzi ⁴⁴, S.A. Rodríguez Ramírez ⁴⁴, K. Røed ¹⁹, R. Rogalev ¹⁴⁰, E. Rogochaya ¹⁴¹,
 T.S. Rogoschinski ⁶⁴, D. Rohr ³², D. Röhrich ²⁰, S. Rojas Torres ³⁵, P.S. Rokita ¹³⁶, G. Romanenko ²⁵,
 F. Ronchetti ³², E.D. Rosas ⁶⁵, K. Roslon ¹³⁶, A. Rossi ⁵⁴, A. Roy ⁴⁸, S. Roy ⁴⁷, N. Rubini ^{51,25},
 J.A. Rudolph ⁸⁴, D. Ruggiano ¹³⁶, R. Rui ²³, P.G. Russek ², R. Russo ⁸⁴, A. Rustamov ⁸¹,
 E. Ryabinkin ¹⁴⁰, Y. Ryabov ¹⁴⁰, A. Rybicki ¹⁰⁷, J. Ryu ¹⁶, W. Rzesz ¹³⁶, B. Sabiu ⁵¹, S. Sadovsky ¹⁴⁰,
 J. Saetre ²⁰, K. Šafařík ³⁵, S. Saha ⁸⁰, B. Sahoo ⁴⁸, R. Sahoo ⁴⁸, S. Sahoo ⁶¹, D. Sahu ⁴⁸, P.K. Sahu ⁶¹,
 J. Saini ¹³⁵, K. Sajdakova ³⁷, S. Sakai ¹²⁵, M.P. Salvan ⁹⁷, S. Sambyal ⁹¹, D. Samitz ¹⁰², I. Sanna ^{32,95},
 T.B. Saramela ¹¹⁰, D. Sarkar ⁸³, P. Sarma ⁴¹, V. Sarritzu ²², V.M. Sarti ⁹⁵, M.H.P. Sas ³², S. Sawan ⁸⁰,
 E. Scapparone ⁵¹, J. Schambach ⁸⁷, H.S. Scheid ⁶⁴, C. Schiaua ⁴⁵, R. Schicker ⁹⁴, F. Schlepper ⁹⁴,
 A. Schmah ⁹⁷, C. Schmidt ⁹⁷, H.R. Schmidt ⁹³, M.O. Schmidt ³², M. Schmidt ⁹³, N.V. Schmidt ⁸⁷,
 A.R. Schmier ¹²², R. Schotter ^{102,129}, A. Schröter ³⁸, J. Schukraft ³², K. Schweda ⁹⁷, G. Scioli ²⁵,
 E. Scomparin ⁵⁶, J.E. Seger ¹⁴, Y. Sekiguchi ¹²⁴, D. Sekihata ¹²⁴, M. Selina ⁸⁴, I. Selyuzhenkov ⁹⁷,
 S. Senyukov ¹²⁹, J.J. Seo ⁹⁴, D. Serebryakov ¹⁴⁰, L. Serkin ⁶⁵, L. Šerksnytė ⁹⁵, A. Sevcenco ⁶³,
 T.J. Shaba ⁶⁸, A. Shabetai ¹⁰³, R. Shahoyan ³², A. Shangaraev ¹⁴⁰, B. Sharma ⁹¹, D. Sharma ⁴⁷,
 H. Sharma ⁵⁴, M. Sharma ⁹¹, S. Sharma ⁷⁶, S. Sharma ⁹¹, U. Sharma ⁹¹, A. Shatat ¹³¹, O. Sheibani ¹¹⁶,
 K. Shigaki ⁹², M. Shimomura ⁷⁷, J. Shin ¹², S. Shirinkin ¹⁴⁰, Q. Shou ³⁹, Y. Sibiriak ¹⁴⁰, S. Siddhanta ⁵²,
 T. Siemarczuk ⁷⁹, T.F. Silva ¹¹⁰, D. Silvermyr ⁷⁵, T. Simantathammakul ¹⁰⁵, R. Simeonov ³⁶, B. Singh ⁹¹,
 B. Singh ⁹⁵, K. Singh ⁴⁸, R. Singh ⁸⁰, R. Singh ⁹¹, R. Singh ⁹⁷, S. Singh ¹⁵, V.K. Singh ¹³⁵,
 V. Singhal ¹³⁵, T. Sinha ⁹⁹, B. Sitar ¹³, M. Sitta ^{133,56}, T.B. Skaali ¹⁹, G. Skorodumovs ⁹⁴,
 N. Smirnov ¹³⁸, R.J.M. Snellings ⁵⁹, E.H. Solheim ¹⁹, J. Song ¹⁶, C. Sonnabend ^{32,97},
 J.M. Sonneveld ⁸⁴, F. Soramel ²⁷, A.B. Soto-hernandez ⁸⁸, R. Spijkers ⁸⁴, I. Sputowska ¹⁰⁷, J. Staa ⁷⁵,
 J. Stachel ⁹⁴, I. Stan ⁶³, P.J. Steffanic ¹²², T. Stellhorn ¹²⁶, S.F. Stiefelmaier ⁹⁴, D. Stocco ¹⁰³,
 I. Storehaug ¹⁹, N.J. Strangmann ⁶⁴, P. Stratmann ¹²⁶, S. Strazzi ²⁵, A. Sturniolo ^{30,53}, C.P. Stylianidis ⁸⁴,
 A.A.P. Suaside ¹¹⁰, C. Suire ¹³¹, M. Sukhanov ¹⁴⁰, M. Suljic ³², R. Sultanov ¹⁴⁰, V. Sumberia ⁹¹,
 S. Sumowidagdo ⁸², M. Szymkowski ¹³⁶, L.H. Tabares ⁷, S.F. Taghavi ⁹⁵, G. Taillepied ⁹⁷,
 J. Takahashi ¹¹¹, G.J. Tambave ⁸⁰, S. Tang ⁶, Z. Tang ¹²⁰, J.D. Tapia Takaki ¹¹⁸, N. Tapus ¹¹³,
 L.A. Tarasovicova ³⁷, M.G. Tarzila ⁴⁵, G.F. Tassielli ³¹, A. Tauro ³², A. Tavira García ¹³¹, G. Tejeda
 Muñoz ⁴⁴, L. Terlizzi ²⁴, C. Terrevoli ⁵⁰, S. Thakur ⁴, D. Thomas ¹⁰⁸, A. Tikhonov ¹⁴⁰,
 N. Tiltmann ^{32,126}, A.R. Timmins ¹¹⁶, M. Tkacik ¹⁰⁶, T. Tkacik ¹⁰⁶, A. Toia ⁶⁴, R. Tokumoto ⁹²,
 S. Tomassini ²⁵, K. Tomohiro ⁹², N. Topilskaya ¹⁴⁰, M. Toppi ⁴⁹, V.V. Torres ¹⁰³, A.G. Torres Ramos ³¹,
 A. Trifiró ^{30,53}, T. Triloiki ⁹⁶, A.S. Triolo ^{32,30,53}, S. Tripathy ³², T. Tripathy ⁴⁷, S. Trogolo ²⁴,
 V. Trubnikov ³, W.H. Trzaska ¹¹⁷, T.P. Trzcinski ¹³⁶, C. Tsolanta ¹⁹, R. Tu ³⁹, A. Tumkin ¹⁴⁰,
 R. Turrisi ⁵⁴, T.S. Tveter ¹⁹, K. Ullaland ²⁰, B. Ulukutlu ⁹⁵, S. Upadhyaya ¹⁰⁷, A. Uras ¹²⁸,
 M. Urioni ¹³⁴, G.L. Usai ²², M. Vala ³⁷, N. Valle ⁵⁵, L.V.R. van Doremalen ⁵⁹, M. van Leeuwen ⁸⁴,
 C.A. van Veen ⁹⁴, R.J.G. van Weelden ⁸⁴, P. Vande Vyvre ³², D. Varga ⁴⁶, Z. Varga ⁴⁶,
 P. Vargas Torres ⁶⁵, M. Vasileiou ⁷⁸, A. Vasiliev ^{I,140}, O. Vázquez Doce ⁴⁹, O. Vazquez Rueda ¹¹⁶,
 V. Vechernin ¹⁴⁰, E. Vercellin ²⁴, S. Vergara Limón ⁴⁴, R. Verma ⁴⁷, L. Vermunt ⁹⁷, R. Vértesi ⁴⁶,
 M. Verweij ⁵⁹, L. Vickovic ³³, Z. Vilakazi ¹²³, O. Villalobos Baillie ¹⁰⁰, A. Villani ²³, A. Vinogradov ¹⁴⁰,
 T. Virgili ²⁸, M.M.O. Virta ¹¹⁷, A. Vodopyanov ¹⁴¹, B. Volkel ³², M.A. Völkl ⁹⁴, S.A. Voloshin ¹³⁷,

G. Volpe ³¹, B. von Haller ³², I. Vorobyev ³², N. Vozniuk ¹⁴⁰, J. Vrláková ³⁷, J. Wan³⁹, C. Wang ³⁹, D. Wang³⁹, Y. Wang ³⁹, Y. Wang ⁶, Z. Wang ³⁹, A. Wegrzynek ³², F.T. Weiglhofer³⁸, S.C. Wenzel ³², J.P. Wessels ¹²⁶, J. Wiechula ⁶⁴, J. Wikne ¹⁹, G. Wilk ⁷⁹, J. Wilkinson ⁹⁷, G.A. Willems ¹²⁶, B. Windelband ⁹⁴, M. Winn ¹³⁰, J.R. Wright ¹⁰⁸, W. Wu³⁹, Y. Wu ¹²⁰, Z. Xiong ¹²⁰, R. Xu ⁶, A. Yadav ⁴², A.K. Yadav ¹³⁵, Y. Yamaguchi ⁹², S. Yang²⁰, S. Yano ⁹², E.R. Yeats¹⁸, Z. Yin ⁶, I.-K. Yoo ¹⁶, J.H. Yoon ⁵⁸, H. Yu¹², S. Yuan²⁰, A. Yuncu ⁹⁴, V. Zaccolo ²³, C. Zampolli ³², F. Zanone ⁹⁴, N. Zardoshti ³², A. Zarochentsev ¹⁴⁰, P. Závada ⁶², N. Zaviyalov¹⁴⁰, M. Zhalov ¹⁴⁰, B. Zhang ^{94,6}, C. Zhang ¹³⁰, L. Zhang ³⁹, M. Zhang ^{127,6}, M. Zhang ⁶, S. Zhang ³⁹, X. Zhang ⁶, Y. Zhang¹²⁰, Z. Zhang ⁶, M. Zhao ¹⁰, V. Zherebchevskii ¹⁴⁰, Y. Zhi¹⁰, D. Zhou ⁶, Y. Zhou ⁸³, J. Zhu ^{54,6}, S. Zhu¹²⁰, Y. Zhu⁶, S.C. Zugravel ⁵⁶, N. Zurlo ^{134,55}

Affiliation Notes

^I Deceased

^{II} Also at: Max-Planck-Institut fur Physik, Munich, Germany

^{III} Also at: Italian National Agency for New Technologies, Energy and Sustainable Economic Development (ENEA), Bologna, Italy

^{IV} Also at: Dipartimento DET del Politecnico di Torino, Turin, Italy

^V Also at: Yildiz Technical University, Istanbul, Türkiye

^{VI} Also at: Department of Applied Physics, Aligarh Muslim University, Aligarh, India

^{VII} Also at: Institute of Theoretical Physics, University of Wroclaw, Poland

^{VIII} Also at: An institution covered by a cooperation agreement with CERN

Collaboration Institutes

¹ A.I. Alikhanyan National Science Laboratory (Yerevan Physics Institute) Foundation, Yerevan, Armenia

² AGH University of Krakow, Cracow, Poland

³ Bogolyubov Institute for Theoretical Physics, National Academy of Sciences of Ukraine, Kiev, Ukraine

⁴ Bose Institute, Department of Physics and Centre for Astroparticle Physics and Space Science (CAPSS), Kolkata, India

⁵ California Polytechnic State University, San Luis Obispo, California, United States

⁶ Central China Normal University, Wuhan, China

⁷ Centro de Aplicaciones Tecnológicas y Desarrollo Nuclear (CEADEN), Havana, Cuba

⁸ Centro de Investigación y de Estudios Avanzados (CINVESTAV), Mexico City and Mérida, Mexico

⁹ Chicago State University, Chicago, Illinois, United States

¹⁰ China Institute of Atomic Energy, Beijing, China

¹¹ China University of Geosciences, Wuhan, China

¹² Chungbuk National University, Cheongju, Republic of Korea

¹³ Comenius University Bratislava, Faculty of Mathematics, Physics and Informatics, Bratislava, Slovak Republic

¹⁴ Creighton University, Omaha, Nebraska, United States

¹⁵ Department of Physics, Aligarh Muslim University, Aligarh, India

¹⁶ Department of Physics, Pusan National University, Pusan, Republic of Korea

¹⁷ Department of Physics, Sejong University, Seoul, Republic of Korea

¹⁸ Department of Physics, University of California, Berkeley, California, United States

¹⁹ Department of Physics, University of Oslo, Oslo, Norway

²⁰ Department of Physics and Technology, University of Bergen, Bergen, Norway

²¹ Dipartimento di Fisica, Università di Pavia, Pavia, Italy

²² Dipartimento di Fisica dell'Università and Sezione INFN, Cagliari, Italy

²³ Dipartimento di Fisica dell'Università and Sezione INFN, Trieste, Italy

²⁴ Dipartimento di Fisica dell'Università and Sezione INFN, Turin, Italy

²⁵ Dipartimento di Fisica e Astronomia dell'Università and Sezione INFN, Bologna, Italy

²⁶ Dipartimento di Fisica e Astronomia dell'Università and Sezione INFN, Catania, Italy

²⁷ Dipartimento di Fisica e Astronomia dell'Università and Sezione INFN, Padova, Italy

²⁸ Dipartimento di Fisica 'E.R. Caianiello' dell'Università and Gruppo Collegato INFN, Salerno, Italy

²⁹ Dipartimento DISAT del Politecnico and Sezione INFN, Turin, Italy

³⁰ Dipartimento di Scienze MIFT, Università di Messina, Messina, Italy

- ³¹ Dipartimento Interateneo di Fisica ‘M. Merlin’ and Sezione INFN, Bari, Italy
³² European Organization for Nuclear Research (CERN), Geneva, Switzerland
³³ Faculty of Electrical Engineering, Mechanical Engineering and Naval Architecture, University of Split, Split, Croatia
³⁴ Faculty of Engineering and Science, Western Norway University of Applied Sciences, Bergen, Norway
³⁵ Faculty of Nuclear Sciences and Physical Engineering, Czech Technical University in Prague, Prague, Czech Republic
³⁶ Faculty of Physics, Sofia University, Sofia, Bulgaria
³⁷ Faculty of Science, P.J. Šafárik University, Košice, Slovak Republic
³⁸ Frankfurt Institute for Advanced Studies, Johann Wolfgang Goethe-Universität Frankfurt, Frankfurt, Germany
³⁹ Fudan University, Shanghai, China
⁴⁰ Gangneung-Wonju National University, Gangneung, Republic of Korea
⁴¹ Gauhati University, Department of Physics, Guwahati, India
⁴² Helmholtz-Institut für Strahlen- und Kernphysik, Rheinische Friedrich-Wilhelms-Universität Bonn, Bonn, Germany
⁴³ Helsinki Institute of Physics (HIP), Helsinki, Finland
⁴⁴ High Energy Physics Group, Universidad Autónoma de Puebla, Puebla, Mexico
⁴⁵ Horia Hulubei National Institute of Physics and Nuclear Engineering, Bucharest, Romania
⁴⁶ HUN-REN Wigner Research Centre for Physics, Budapest, Hungary
⁴⁷ Indian Institute of Technology Bombay (IIT), Mumbai, India
⁴⁸ Indian Institute of Technology Indore, Indore, India
⁴⁹ INFN, Laboratori Nazionali di Frascati, Frascati, Italy
⁵⁰ INFN, Sezione di Bari, Bari, Italy
⁵¹ INFN, Sezione di Bologna, Bologna, Italy
⁵² INFN, Sezione di Cagliari, Cagliari, Italy
⁵³ INFN, Sezione di Catania, Catania, Italy
⁵⁴ INFN, Sezione di Padova, Padova, Italy
⁵⁵ INFN, Sezione di Pavia, Pavia, Italy
⁵⁶ INFN, Sezione di Torino, Turin, Italy
⁵⁷ INFN, Sezione di Trieste, Trieste, Italy
⁵⁸ Inha University, Incheon, Republic of Korea
⁵⁹ Institute for Gravitational and Subatomic Physics (GRASP), Utrecht University/Nikhef, Utrecht, Netherlands
⁶⁰ Institute of Experimental Physics, Slovak Academy of Sciences, Košice, Slovak Republic
⁶¹ Institute of Physics, Homi Bhabha National Institute, Bhubaneswar, India
⁶² Institute of Physics of the Czech Academy of Sciences, Prague, Czech Republic
⁶³ Institute of Space Science (ISS), Bucharest, Romania
⁶⁴ Institut für Kernphysik, Johann Wolfgang Goethe-Universität Frankfurt, Frankfurt, Germany
⁶⁵ Instituto de Ciencias Nucleares, Universidad Nacional Autónoma de México, Mexico City, Mexico
⁶⁶ Instituto de Física, Universidade Federal do Rio Grande do Sul (UFRGS), Porto Alegre, Brazil
⁶⁷ Instituto de Física, Universidad Nacional Autónoma de México, Mexico City, Mexico
⁶⁸ iThemba LABS, National Research Foundation, Somerset West, South Africa
⁶⁹ Jeonbuk National University, Jeonju, Republic of Korea
⁷⁰ Johann-Wolfgang-Goethe Universität Frankfurt Institut für Informatik, Fachbereich Informatik und Mathematik, Frankfurt, Germany
⁷¹ Korea Institute of Science and Technology Information, Daejeon, Republic of Korea
⁷² KTO Karatay University, Konya, Turkey
⁷³ Laboratoire de Physique Subatomique et de Cosmologie, Université Grenoble-Alpes, CNRS-IN2P3, Grenoble, France
⁷⁴ Lawrence Berkeley National Laboratory, Berkeley, California, United States
⁷⁵ Lund University Department of Physics, Division of Particle Physics, Lund, Sweden
⁷⁶ Nagasaki Institute of Applied Science, Nagasaki, Japan
⁷⁷ Nara Women’s University (NWU), Nara, Japan
⁷⁸ National and Kapodistrian University of Athens, School of Science, Department of Physics , Athens, Greece
⁷⁹ National Centre for Nuclear Research, Warsaw, Poland
⁸⁰ National Institute of Science Education and Research, Homi Bhabha National Institute, Jatni, India
⁸¹ National Nuclear Research Center, Baku, Azerbaijan

- ⁸² National Research and Innovation Agency - BRIN, Jakarta, Indonesia
⁸³ Niels Bohr Institute, University of Copenhagen, Copenhagen, Denmark
⁸⁴ Nikhef, National institute for subatomic physics, Amsterdam, Netherlands
⁸⁵ Nuclear Physics Group, STFC Daresbury Laboratory, Daresbury, United Kingdom
⁸⁶ Nuclear Physics Institute of the Czech Academy of Sciences, Husinec-Řež, Czech Republic
⁸⁷ Oak Ridge National Laboratory, Oak Ridge, Tennessee, United States
⁸⁸ Ohio State University, Columbus, Ohio, United States
⁸⁹ Physics department, Faculty of science, University of Zagreb, Zagreb, Croatia
⁹⁰ Physics Department, Panjab University, Chandigarh, India
⁹¹ Physics Department, University of Jammu, Jammu, India
⁹² Physics Program and International Institute for Sustainability with Knotted Chiral Meta Matter (SKCM2), Hiroshima University, Hiroshima, Japan
⁹³ Physikalisches Institut, Eberhard-Karls-Universität Tübingen, Tübingen, Germany
⁹⁴ Physikalisches Institut, Ruprecht-Karls-Universität Heidelberg, Heidelberg, Germany
⁹⁵ Physik Department, Technische Universität München, Munich, Germany
⁹⁶ Politecnico di Bari and Sezione INFN, Bari, Italy
⁹⁷ Research Division and ExtreMe Matter Institute EMMI, GSI Helmholtzzentrum für Schwerionenforschung GmbH, Darmstadt, Germany
⁹⁸ Saga University, Saga, Japan
⁹⁹ Saha Institute of Nuclear Physics, Homi Bhabha National Institute, Kolkata, India
¹⁰⁰ School of Physics and Astronomy, University of Birmingham, Birmingham, United Kingdom
¹⁰¹ Sección Física, Departamento de Ciencias, Pontificia Universidad Católica del Perú, Lima, Peru
¹⁰² Stefan Meyer Institut für Subatomare Physik (SMI), Vienna, Austria
¹⁰³ SUBATECH, IMT Atlantique, Nantes Université, CNRS-IN2P3, Nantes, France
¹⁰⁴ Sungkyunkwan University, Suwon City, Republic of Korea
¹⁰⁵ Suranaree University of Technology, Nakhon Ratchasima, Thailand
¹⁰⁶ Technical University of Košice, Košice, Slovak Republic
¹⁰⁷ The Henryk Niewodniczanski Institute of Nuclear Physics, Polish Academy of Sciences, Cracow, Poland
¹⁰⁸ The University of Texas at Austin, Austin, Texas, United States
¹⁰⁹ Universidad Autónoma de Sinaloa, Culiacán, Mexico
¹¹⁰ Universidade de São Paulo (USP), São Paulo, Brazil
¹¹¹ Universidade Estadual de Campinas (UNICAMP), Campinas, Brazil
¹¹² Universidade Federal do ABC, Santo Andre, Brazil
¹¹³ Universitatea Nationala de Stiinta si Tehnologie Politehnica Bucuresti, Bucharest, Romania
¹¹⁴ University of Cape Town, Cape Town, South Africa
¹¹⁵ University of Derby, Derby, United Kingdom
¹¹⁶ University of Houston, Houston, Texas, United States
¹¹⁷ University of Jyväskylä, Jyväskylä, Finland
¹¹⁸ University of Kansas, Lawrence, Kansas, United States
¹¹⁹ University of Liverpool, Liverpool, United Kingdom
¹²⁰ University of Science and Technology of China, Hefei, China
¹²¹ University of South-Eastern Norway, Kongsberg, Norway
¹²² University of Tennessee, Knoxville, Tennessee, United States
¹²³ University of the Witwatersrand, Johannesburg, South Africa
¹²⁴ University of Tokyo, Tokyo, Japan
¹²⁵ University of Tsukuba, Tsukuba, Japan
¹²⁶ Universität Münster, Institut für Kernphysik, Münster, Germany
¹²⁷ Université Clermont Auvergne, CNRS/IN2P3, LPC, Clermont-Ferrand, France
¹²⁸ Université de Lyon, CNRS/IN2P3, Institut de Physique des 2 Infinis de Lyon, Lyon, France
¹²⁹ Université de Strasbourg, CNRS, IPHC UMR 7178, F-67000 Strasbourg, France, Strasbourg, France
¹³⁰ Université Paris-Saclay, Centre d'Etudes de Saclay (CEA), IRFU, Département de Physique Nucléaire (DPhN), Saclay, France
¹³¹ Université Paris-Saclay, CNRS/IN2P3, IJCLab, Orsay, France
¹³² Università degli Studi di Foggia, Foggia, Italy
¹³³ Università del Piemonte Orientale, Vercelli, Italy
¹³⁴ Università di Brescia, Brescia, Italy

¹³⁵ Variable Energy Cyclotron Centre, Homi Bhabha National Institute, Kolkata, India

¹³⁶ Warsaw University of Technology, Warsaw, Poland

¹³⁷ Wayne State University, Detroit, Michigan, United States

¹³⁸ Yale University, New Haven, Connecticut, United States

¹³⁹ Yonsei University, Seoul, Republic of Korea

¹⁴⁰ Affiliated with an institute covered by a cooperation agreement with CERN

¹⁴¹ Affiliated with an international laboratory covered by a cooperation agreement with CERN.